HHS Public Access

Author manuscript

Nat Cardiovasc Res. Author manuscript; available in PMC 2022 November 16.

Published in final edited form as:

Nat Cardiovasc Res. 2022 May ; 1(5): 518–528. doi:10.1038/s44161-022-00064-2.

Syndecan-2 selectively regulates VEGF-induced vascular permeability

F Corti[1], **E Ristori**[1], **F Rivera-Molina**[2], **D Toomre**[2], **J Zhang**[1], **J Mihailovic**[3], **ZW Zhuang**[1], **M. Simons**[1]

[1]Yale Cardiovascular Research Center Department of Internal Medicine, Yale University School of Medicine, New Haven, CT 06511, USA

[2]Department of Cell Biology, Yale University School of Medicine, New Haven, CT 06511, USA

[3]Department of Radiology, Yale University School of Medicine, New Haven, CT 06511, USA

Abstract

Vascular endothelial growth factor (VEGF)- driven increase in vascular permeability is a key feature of many disease states associated with inflammation and ischemic injury, contributing significantly to morbidity and mortality in these settings. Despite its importance, no specific regulators that preferentially control VEGF-dependent increase in permeability versus its other biological activities, have been identified. Here we report that a proteoglycan Syndecan-2 (Sdc2) regulates the interaction between a transmembrane phosphatase DEP1 and VEGFR2 by controlling cell surface levels of DEP1. In the absence of Sdc2 or the presence of an antibody that blocks Sdc2-DEP1 interaction, increased plasma membrane DEP1 levels promote selective dephosphorylation of the VEGFR2 Y951 site that is involved in permeability control. Either an endothelial-specific Sdc2 deletion or a treatment with an anti-Sdc2 antibody result in a highly significant reduction in stroke size due to a decrease in intracerebral edema

Dynamic control of vascular permeability is central to homeostasis maintenance. While under normal conditions most vascular beds do not allow free movement of solute and cells, this can rapidly change in response to both physiological and pathological stimuli [1–3]. Vascular endothelial growth factor (VEGF) is one of the most potent inducers of permeability. VEGF levels increase dramatically in settings of acute ischemic injury or chronic inflammation due to the presence of inflammatory cells capable of producing the growth factor, with a strong contribution of inflammation-induced edema attributable to VEGF activity [4–7]. VEGF exerts its permeability-inducing effects by binding to its

Address correspondence to: Prof. Michael Simons, Yale Cardiovascular Research Center, 300 George St, Rm 753, New Haven, CT 06511, michael.simons@yale.edu, phone: 203-737-4643.

Author Contribution Statement

F.C. designed and performed experiments, analyzed data and wrote manuscript. E.R. designed/performed experiments and analyzed data. R-M.F. performed experiments and analyzed data, T.D. designed experiments and analyzed data, J.Z., Z.W.Z, J.M, performed experiments, M.S. designed experiments, analyzed data and wrote the manuscript.

Competing Interests Statement

The authors declare no competing interests.

principal signaling receptor, VEGFR2, leading to phosphorylation of tyrosine Y951 (human equivalent of mouse Y949) and activation of the Src cascade [8–11]. The latter event promotes disassembly of adherens and tight junctions with the resultant increase in vascular leakiness [12–16].

VEGF belongs to a family of heparin-binding growth factors and its interactions with VEGFR2 is governed by the presence of heparan sulfate (HS) chains-carrying proteoglycans on the cell surface [17,18]. One of these proteoglycans, a transmembrane protein Syndecan-2 (Sdc2), has been recently shown to carry HS chain that preferentially bind $VEGFA_{165}$ [19]. To gain understanding of the role of Sdc2 in VEGF biology, we undertook a study of its function in regulation of vascular permeability.

We first examined the effect of Sdc2 knockout on VEGF signaling responses in primary mouse endothelial cells (ECs). As expected, there was a mild reduction in phosphorylation of the VEGFR2 Y1175 kinase site (Y1173 in mouse) that was previously traced to a reduction in $VEGFA_{165}$-VEGFR2 binding in the absence of Sdc2 HS chains [19] (Fig. 1a,b). Since HS chains facilitate VEGFR2 occupation by $VEGFA_{165}$, we expected other VEGFR2 phosphosites to be equally affected in Sdc2 null cell ($Sdc2^{-/-}$). However, while there was a comparable decline in VEGFR2 Y1059 (Y1057 in mouse) phosphorylation (~25% decrease for Y1059 and Y1175 at 5 minutes post-$VEGFA_{165}$ stimulation) (Fig. 1a,c), there was a larger reduction of Y951 (~40% decrease at 5 minutes post-$VEGFA_{165}$ stimulation) (Fig. 1a,d) suggesting that Sdc2 may regulate VEGFR2 activation in phosphotyrosine-specific manner. To test whether Sdc2 core protein could be play a role in such mechanism, we measured VEGFR2 activation following treatment with non-HS binding $VEGFA_{121}$[20]. In contrast to $VEGFA_{165}$ stimulation, there was no significant reduction in either Y1059 or Y1175 phosphorylation (Fig. 1f,g–h). However, there was a 40% reduction in Y951 phosphorylation (Fig. 1f,i) that was similar in magnitude to that seen with $VEGFA_{165}$. Src activation is the major downstream event following VEGFR2 Y951 phosphorylation[9]. Accordingly, we found that VEGFA-induced Src activation was impaired in $Sdc2^{-/-}$ ECs in response to both $VEGFA_{165}$ and $VEGFA_{121}$ (Fig, 1a,e and Fig. 1f,j). Sdc2 knockdown in human umbilical venous endothelial cells (HUVECs) confirmed decreased Y951 phosphorylation and reduced Src activation following $VEGFA_{165}$ and $VEGFA_{121}$ stimulation (Extended Data Fig. 1a,b)

Phosphorylation of VEGFR2 Y951 site is known to activate the Tsad-Src-VE-cadherin pathway, which controls junctional stability and permeability [21]. To test if Sdc2 knockout affects the permeability response we used Miles Assay [22]. Mice with a global Sdc2 deletion ($Sdc2^{-/-}$), endothelial-specific deletion of Sdc2 (obtained by crossing $Cdh5CreR^{T2}$ line [23] with $Sdc2^{fl/fl}$, here by referred to as $Sdc2^{iECKO}$) or wildtype controls were injected intradermally with either $VEGFA_{165}$, $VEGFA_{121}$ or histamine and the extent of vascular permeability in the skin was measured by Evans Blue dye extravasation. Both VEGFs induced a much smaller extent of dye extravasation in $Sdc2^{-/-}$ (Fig. 1k–n) and $Sdc2^{iECKO}$ mice (Extended Data Fig. 1c) compared to wild type control mice. At the same time, Sdc2 knockout had no effect on the vascular permeability response to histamine (Fig. 1o,p). We also assessed baseline vascular integrity of $Sdc2^{-/-}$ mice by measuring Evans Blue

extravasation in various organs in the absence of VEGF stimulation. In all cases, basal permeability in these mice was comparable to wild type controls (Extended Data Fig. 1d).

To investigate the molecular basis of reduced Y951 phosphorylation and a corresponding reduction in VEGF-induced permeability in $Sdc2^{-/-}$ and $Sdc2^{iECKO}$ mice, we studied expression of key members of VEGF signaling cascade and its regulators, including membrane receptor phosphatases VEPTP [24] and DEP1[25,26], and the intracellular ER-anchored PTP1B [27]. Sdc2 knockout had no effect on total cellular levels of VEGF receptors (VEGFR1, VEGFR2 and Neuropilin-1 (Nrp1)), the adhesion protein VE-cadherin and the three phosphatases (Fig. 2 a). However, examination of the cell surface levels of these proteins demonstrated a significant increase in DEP1 levels in $Sdc2^{-/-}$ ECs (Fig. 2 b, c). Increased DEP1 surface level was confirmed in HUVEC following Sdc2 knockdown (Extended Data Fig. 1e,f).

To check if this increase in cell surface DEP1 could account for a selective increase in VEGFR2 Y951 dephosphorylation, we transduced HUVECs with an adenovirus carrying the DEP1 expression construct. Overexpression of DEP1 reduced $VEGFA_{165}$-induced Y951 but had minimal effect on Y1059 or Y1175 sites phosphorylation (Fig. 2d –f).

To show that this effect is DEP1-specific, we performed a knockdown of the three phosphatases known to affect VEGFR2 signaling [28] and measured their impact on the extent of $VEGFA_{165}$-induced VEGFR2 phosphorylation. In agreement with published studies [29], PTP1b knockdown preferentially increased Y1175 phosphorylation, leaving Y951 site phosphorylation unchanged (Fig. 2g, j), while VEPTP knockdown increased phosphorylation of all examined VEGFR2 sites (Fig. 2 h,j). In contrast, DEP1 knockdown preferentially increased Y951 phosphorylation while phosphorylation levels of Y1059 and Y1175 were minimally affected (Fig. 2 i,j).

DEP1 is a transmembrane phosphatase enriched at cell-cell contacts in ECs and other cell types[30,31], which interacts with various components of the adherens junction complex (e.g. VE-cadherin, p120-catenin, and β-catenin)[32]. Indeed, we observed that DEP1 was mostly localized at cell junctions of confluent ECs (Extended Data Fig. 2a). Both Sdc2 and DEP1 are expressed at the cell surface (Extended Data Fig. 2b) and can engage in a direct interaction[33], while Sdc2 HS chains mediate formation of a ternary complex with $VEGFA_{165}$ and VEGFR2 following $VEGFA_{165}$ stimulation in endothelial cells. Therefore, we hypothesized that DEP1 surface level are linked to endocytosis of the $VEGFA_{165}$-VEGFR2-Sdc2- ternary complex as it gets internalized in tandem with Sdc2. The absence of Sdc2 would reduce DEP1 cell entry thereby increasing its plasma membrane levels and decreasing VEGFR2 Y951 site phosphorylation thereby reducing permeability.

To test this possibility, we first evaluated whether Sdc2 and Dep1 internalize with a time course similar to VEGFR2. $VEGFA_{165}$ stimulation in HUVEC led to a prompt internalization of all three proteins with a similar kinetics as shown by decreasing cell surface levels (Fig. 3a,b). Furthermore, SIM analysis shows that $VEGFA_{165}$ stimulation led to a higher colocalization of Sdc2 (Fig. 3c) and DEP1 (Fig. 3d) with VEGFR2 in Rab5+ endosomes, indicating that Sdc2 and DEP1 internalization follows a clathrin-mediated

endocytic process like VEGFR2 [29,34]. SIM images also revealed copresence of Sdc2/DEP1 in Rab5+ and VEGFR2+ endosomal structures (Extended Data Fig. 2c–f) suggesting a molecular link between Sdc2, DEP1 and VEGFR2.

To assess whether Sdc2 is required for DEP1 internalization, we isolated primary endothelial cells from wild type and Sdc2 $^{-/-}$ mice and measured DEP1 internalization after $VEGFA_{165}$ stimulation. We observed that DEP1, but not VEGFR2, internalization was greatly impaired in the absence of Sdc2 (Fig. 3e–h). We then used immunofluorescence to examine DEP1 and VEGFR2 internalization in response to VEGF stimulation wild type and $Sdc2^{-/-}$ primary ECs transduced with comparable level of surface HA-tagged DEP1. The loss of Sdc2 led to a significant decrease of internalized DEP1 that co-localize in VEGFR2+ endocytic complexes (Fig. 3i,j).

We also examined whether DEP1 undergoes constitutive endocytosis in the absence of added $VEGFA_{165}$ and whether it is dependent from Sdc2. HUVEC kept in the VEGFA-free media displayed a degree of constitutive DEP1 internalization, which was significantly reduced after Sdc2 knockdown (Extended Data Fig. 2g,h). Moreover, confocal images of HUVECs showed the presence of DEP1-SDC2 complexes in Rab5+ endosomal compartments in the absence of VEGFA stimulation (Extended Data Fig. 2i).

Overall, these results suggest that a Sdc2-DEP1 interaction is necessary for DEP1 internalization. To formally prove this hypothesis, we generated a polyclonal antibody against DEP1-binding domain of Sdc2 [33] mouse sequence (Extended Data Fig. 3a) in the attempt to disrupt Sdc2-DEP1 association. Validation of this anti-Sdc2 polyclonal antibody (Sdc2 pAb) confirmed specific binding to Sdc2 but not Syndecan-4 (Sdc4) (Extended Data Fig. 3b). Furthermore, HUVEC transduced with mouse Sdc2 (V5-Tag) and human DEP1 (HA-tag) constructs followed by treatment with the Sdc2 pAb showed a marked reduction in Sdc2/DEP1 association (Fig. 3k).

We then tested the ability of the Sdc2 pAb to block $VEGFA_{165}$-induced DEP1 internalization in mouse brain endothelial cells (bEnd.3 cells). Preincubation of bEnd.3 cells with Sdc2 pAb (1 hour) prevented $VEGFA_{165}$-induced DEP1 internalization compared to IgG treatment (Fig. 3l,m,o). In agreement with decreased Y951-Src activation, internalization of VE-Cadherin was also reduced upon treatment with Sdc2 pAb (Fig 3 l,m). However, VEGFR2 internalization was not affected by treatment with Sdc2 pAb (Fig. 3l,m,n). In line with these findings, Sdc2 pAb preferentially led to decreased phosphorylation of VEGFR2 Y951 vs Y1175 (Fig 3p,q). Finally, to evaluate the functional consequence of the Sdc2 pAb treatment, we studied the effect of this pAb treatment on bEnd.3 cells *in vitro*. In agreement with a strong decrease in Y951 activation, cells treated with the Sdc2 pAb showed significant inhibition of VEGFA-induced decline in Trans-Endothelial Electrical Resistance (TEER) (Fig. 3r), a measure of endothelial barrier integrity which normally correlate with changes in vascular permeability *in vivo* [35]. In contrast, $VEGFA_{165}$-induced proliferation and migration were not affected by Sdc2 pAb treatment (Extended Data Fig.3c–e)

VEGFA-induced permeability plays a pathogenic role in a number of disease processes [36,37]. In particular, a rapid rise in $VEGFA_{165}$ levels following a stroke is thought to destabilize the blood-brain barrier leading to a peri-infarct edema (vasogenic edema) and unregulated entrance into the brain parenchyma of blood-borne substances that further increase the damage, leading to a substantial increase in the final infarct size [38–40]. Since $Sdc2^{-/-}$ mice display a reduced permeability in response to VEGFA, we set out to test if this translates into reduced stroke size in these mice. To this end, we induced an acute stroke in $Sdc2^{-/-}$ and wild type (WT) mice with a permanent ligation of the distal middle cerebral artery (MCA) via craniectomy [41]. Morphometric evaluation of the infarct size 24 hours after ligation using TTC live staining demonstrated a significant 35% reduction in the stroke size (Fig. 4a,b). To assess whether reduced infarct size is due Sdc2 deletion in endothelial cells, we repeated the same stroke model in $Sdc2^{iECKO}$ mice (Extended Data Fig. 3f,g). Here, we observed a similar reduction in infarct size as in the global $Sdc2^{-/-}$ mice suggesting that reduced endothelial permeability is the main driver of the neuroprotective effect of Sdc2 deletion.

Finally, we set out to evaluate the therapeutic potential of preventing VEGF-induced edema formation by blocking the Sdc2-DEP1 interaction with our validated antibody described above (Sdc2 pAb). First, we checked the effectiveness of the Sdc2 pAb in modulating skin permeability. An intravenous injection of the blocking Sdc2 pAb antibody abolished VEGFA-induced permeability in the mouse skin mice compared to IgG controls (Fig. 4c,d) However, Sdc2 pAb did not affect the skin permeability response to histamine (Fig 4 e,f) nor inhibited $VEGFA_{165}$-induced angiogenesis in a cornea pocket *assay* (Fig. 4g, h).

We then tested whether the Sdc2 blocking-antibody could confer neuroprotection in the same mouse stroke model as used in Sdc2 null mice. Indeed, I.V. injection either before (Fig. 4i, j) or after MCA ligation (Fig. 4k, l) resulted in a significant reduction in the infarct size after 24hrs. Finally, we found that treatment of Sdc2 null mice with Sdc2 pAb did not alter stroke size (Extended Data Fig. 3h–i), indicating antibody specificity towards Sdc2 function.

To further confirm that the neuroprotective effect is due to Sdc2 pAb ability to inhibit vasogenic edema, we used multi modal magnetic resonance imaging (MRI) to quantify the volume of the edema in IgG- and Sdc2 pAb-treated mice. To this end, we performed a transient occlusion of the middle cerebral artery (45 minutes occlusion followed by reperfusion) and then injected either the Sdc2 pAb or a control IgG 30 minutes post-reperfusion. Brain MRI scanning was then performed 24 hrs later. Compartmentalization analysis of MRI images (Extended Data Fig. 4 and method section for mathematical details) allowed to define affected areas as follow: ischemic stroke core (white), penumbra (light green) and extracellular vasogenic edema (dark green) (Fig. 4m). Quantification of these parameters revealed that mice receiving Sdc2 pAb developed significantly less vasogenic edema compared to IgG treated-mice, indicating that Sdc2 pAb treatment has an anti-edematous effect in ischemic stroke (Fig.4n)

DISCUSSION

These results describe a novel pathway selectively regulating VEGF-induced vascular permeability. The key control point is Sdc2-dependent endocytosis of DEP1 (Fig. 5). The two proteins normally exist in a heteromeric complex on the endothelial cell surface with Sdc2 internalization triggering DEP1 endocytosis thereby reducing its ability to dephosphorylate VEGFR2 Y951 site at the cell surface. In the absence of Sdc2, DEP1 inability to internalize leads to an increased stochiometric ratio of DEP1/VEGFR2 at the cell surface, selective dephosphorylation of the VEGFR2 Y951 site, and reduction in permeability response. The surprising specificity of DEP1 for Y951 may be due to the amino acid sequence flanking the site that closely resemble DEP1 consensus binding site (Fig. 5b).

Interestingly, we observed a more selective defect of Y951 phosphorylation with $VEGFA_{121}$ stimulation compared to $VEGFA_{165}$. This is likely due to the fact that $VEGFA_{165}$ but not $VEGFA_{121}$ requires Sdc2 HS chains to efficiently occupy VEGFR2[19]. Consequently, $VEGFA_{165}$- but not $VEGFA_{121}$-induced VEGFR2 phosphorylation in Sdc2 null endothelial cells is somewhat reduced globally (~25%) in other phospho-tyrosine sites. At the same time, $VEGFA_{121}$- induced VEGFR2 phosphorylation, which is HS independent, is reduced only on the Y951 site, further demonstrating a direct causal relationship between plasma membrane levels of DEP1 and VEGFR2 Y951 phosphorylation. In agreement with such explanation, we found that increasing DEP1 surface level through overexpression led to a selective decrease in VEGFR2 Y951 phosphorylation in response to $VEGFA_{165}$ stimulation (Figure 2d).

In addition, VEGFR2 Y951 phosphorylation in unstimulated Sdc2 null endothelial cells appears to decrease even below baseline following stimulation with VEGFA. Baseline VEGFR2 phosphorylation can be the consequence of ligand-independent activation mechanisms such the effect of fluid shear stress[42] and direct Src activity toward VEGFR2 tyrosine sites[43]. Thus, one possible explanation for Y951 decrease below baseline following VEGFA stimulation is that once VEGFR2 starts to internalize it is displaced from transactivation mechanisms. Another possibility is simply that once VEGFR2 gets inside the cells, it is exposed to intracellular phosphatases[28] that further decrease Y951 phosphorylation below baseline.

Mechanistically, Sdc2 forms a heteromeric complex with DEP1 likely due to a direct binding of the latter to Sdc2[33]. $VEGFA_{165}$ binding to Sdc2 HS chains brings Sdc2, along with its DEP1 partner, into the $VEGFA_{165}$-VEGFR2 complex. VEGFA-triggered internalization of VEGFR2 pulls Sdc2 and its DEP1 partner along. In absence of Sdc2, DEP1 is not internalized with the VEGFA/VEGFR2 complex resulting its accumulation on the plasma membrane and increased VEGFR2 Y951 dephosphorylation.

Syndecan-2, as all other syndecans, can undergo shedding on the cell surface [44] and its shed extracellular domain can interact with DEP1[33]. In this study, we have not specifically investigated whether Sdc2 shedding is involved in regulation of permeability and we cannot exclude a possibility that this process may also play a role in modulation of DEP1 surface

levels and VEGFR2 dephosphorylation. A recent study reported that syndecan-4 (Sdc4) can induce activation and internalization of VE-Cadherin [45]. How Sdc4 does that and whether this modulation is involved in a specific regulation of VEGFA-induced permeability is not clear. Since Sdc2 and Sdc4 can form heterodimer [46], it is also possible that Sdc4 can modulate Sdc2 distribution at the cell membrane.

Importantly, Sdc2-DEP1 interaction can be exploited for therapeutic purposes: an antibody blocking this protein-protein interaction leads to an increase in cell surface DEP1 levels and a decreased permeability response to VEGFA. In functional terms, this was effective as the Sdc2 knockout, resulting in a highly significant reduction in stroke size. The Sdc2 polyclonal antibody we employed (Sdc2 pAb), disrupts Sdc2-DEP1 interaction by targeting the DEP1-binding motif on the Sdc2 core protein. This does not affect $VEGFA_{165}$ binding to Sdc2 HS chains which are required for full VEGFR2 activation and angiogenesis. As the result, the only impaired VEGFR2 signaling pathway is VEGFR2-Y951-dependent phosphorylation activation of Src signaling and vascular permeability [3,10] with minimal interference to other VEGFA biological effects. In agreement with these findings, a selective inactivation of Y951-Src pathway in a mouse genetic model (VEGFR2 Y951F mutation) results in live mice without angiogenenic defects but with a specific impairment of VEGFA-induced vascular permeability [21].

No changes in basal permeability were seen in Sdc2 null mice in this study, implying that DEP1/VEGFR2 interaction does not regulate this process. On the other hand, conditions that lead with increased endothelial Sdc2 expression such as inflammation and hypoxia [47–49] may also increase basal permeability since Sdc2 HS chains can sensitize VEGFR2 activation [19]. Thus, increasing the level of Sdc2 HS chains might ultimately lead to enough VEGFR2 activation to alter vascular permeability even under physiological $VEGFA_{165}$ concentrations.

Finally, DEP1 has been shown to modulate endothelial barrier function by dephosphorylation of various proteins of adherens and tight junctions (e.g. VE-Cadherin, Occludin, p120 and gamma-catenin, beta-catenin)[32]. Thus, we cannot exclude that a direct effect of higher surface DEP1 on junction proteins may contribute to the observed permeability phenotype in Sdc2 null mice due to one of these interactions. Additionally, if the absence of Sdc2 results in changes in junctional phosphorylation, it is possible that other biological process such as leukocyte transmigration and shear stress sensing may also be affected in Sdc2 null mice.

In summary, Sdc2 is a regulator of VEGF-dependent vascular permeability response that acts by controlling cell surface DEP1 levels thereby enabling a selective regulation of a specific VEGF signaling pathway. This unique feature of Sdc2-dependent regulation of permeability makes it an appealing therapeutic target for treatment of conditions such as stroke [39,40] where suppression of permeability needs to be coupled with preservation of the vasculature and VEGFA neuroprotective and neurogenic effects [36,50,51].

Methods

List of antibodies and growth factors.

List of antibodies with application and dilutions (IHC, immunohistochemistry; WB; western blot): pVEGFR2 Y1175 (WB 1:1000, Cell Signaling #2478), pVEGFR2 Y1059 (for HUVEC, WB 1:1000, Cell Signaling #3817,), pVEGFR2 Y1059 (for mouse ECs, WB 1:1000, EMD Millipore #ABS553), pVEGFR2 Y951 (WB 1:1000, Cell Signaling #4991), VEGFR2 total (WB 1:1000, Cell Signaling #2479), VE-Cad (for HUVEC, WB 1:200, Santa Cruz #sc-9989 (F-8)), VE-Cad (for mouse ECs, WB 1:500, BD Pharmingen #555289), mouse Sdc2 (WB 1:200, R&D #AF6585 - polyclonal raised against mouse Sdc2 ED), human Sdc2 (WB 1:200, R&D # AF2965, polyclonal raised against mouse human ED), mouse PTP1b (WB 1:200, Santa Cruz #sc-1718-R (N19-R)), human PTP1b (WB 1:500, BD Pharmingen #610139), VEPTP (VE-PTP-C pAb69 and VE-PTP 1–8 pAb70 were gifts from Prof. Dietmar Vestweber, Max Plank Institute for Molecular Biomedicine, Münster, Germany), DEP1 (WB 1:200, Santa Cruz #sc-21761 (143–41)) NRP1 (WB 1:1000, Cell signaling #3725,), HA-tag (WB 1:1000, Cell signaling #3724), rabbit anti-Rab5 (Cell Signaling, #3547, IHC 1:200); goat anti-VEGFR2 (R&D, #AF357, IHC 1:100); mouse anti-HA.11 (Covance, #MMS-101P, IHC 1:200); rabbit anti-HA (Cell signaling, #3724, IHC 1:200); rabbit anti-VE-cadherin (Cell Signaling, #2500, IHC 1:200); goat anti-mouse VE-cadherin (R&D Systems, #AF1002, IHC 1:100); rat anti-mouse Flk1 (BD, #555307, IHC 1:100).

List of Growth factors:

$VEGFA_{165}$ (R&D #293-VE-010), $VEGFA_{121}$ (R&D #4644-VS-010).

Animal Studies

All mouse experimental protocols have been approved by the Institutional Animal Care & Use Committee (IACUC) at Yale University. The authors have complied with all relevant animal testing and research ethical regulations. All transgenic mice used in this study has been previously described[19]. Sdc2 Knockout-first transgenic mice (Sdc2tm1a(KOMP)Wtsi), Sdc2 null mice ($Sdc2^{-/-}$), Sdc2 conditional transgenic mice ($Sdc2^{fl/fl}$), Sdc2 endothelial-specific knockout ($sdc2^{icdh5}$). All animals were back-crossed at least 10 generation to a C57Black6/J strain. For this study male mice (Specie: *mus musculus)* were used between age 9–15 weeks old.

Detection of syndecan expression by western blotting

Sdc2 detection in mouse ECs and HUVEC: heparinase pre-treatment is required to unveil epitopes on core protein and remove non-specific sugar epitopes. Briefly, confluent ECs on 6 cm tissue culture dishes were rinsed twice with DPBS. Cells were then incubated with 1.5 ml of serum-free media (Opti-MEM, Thermo Fisher) containing 2 Unit of Heparinase I-III (Sigma-Aldrich, #H2519 and #H8891) and 1 Unit of Heparinase II (Sigma-Aldrich, #H6512). After 2.5 hours digestion at 37 °C under gentle agitation, cells were washed three times with ice-cold PBS and lysed in 250ul of RIPA buffer. Samples were then analyzed by western blot. Specific Sdc2 core protein bands can be observed at ~37 KDa and ~48 KDa.

Additional specific band smears, due to Sdc2 glycosylation isoforms (50–250 KDa), can be sometimes observed if heparinase digestion of HS chains is incomplete.

HA-Tag syndecans: heparinase pre-treatment is not required. HA detection reveals naked core proteins in a dimeric form and additional higher molecular weight smear bands due to glycosylation isoforms.

Cell culture and mouse ECs isolation.

Human Umbilical Vein Endothelial Cells (HUVEC) were obtained from Yale VBT tissue-culture core laboratory at Passage 1 and maintained in complete EGM-2 MV medium (LONZA). HUVEC were used for experiments between P2 and P6. Primary mouse ECs were isolated as previously described [52]. Briefly, 4 hearts or lungs were harvested, finely minced with scissors and digested (37°C for 45 minutes under gentle agitation) with 25 ml of 1.5 mg/ml Collagenase/Dispase® solution for Heart (Sigma-Aldrich #10269638001) or 2 mg/ml Collagenase Type I (Sigma-Aldrich #C0130). The crude preparation was triturated passing it 10 times through a cannula needle, filtered on a 70-μM sterile cell strainer, and spun at 400g for 10 minutes. Pellet was resuspended in 2 ml of 0.1% BSA and 50μl magnetic dynabeads (Thermo Fisher #11035) pre-coated overnight with anti-mouse CD31 (BD Pharmingen ™ #553370) were added for ECs positive selection. Selection was carried out for 25 minutes at room temperature under slow rotation. The bead-bound cells were recovered with a magnetic separator and washed 5 times with DMEM containing 10% FBS. Cells were finally resuspended in 10 ml of complete DMEM medium (20%FBS with ECGS and antibiotics) and seeded onto gelatin-precoated 10 cm plates. bEnd.3 cell line was purchased from ATCC (CRL-2299™) and maintained in DMEM with 10%FBS and streptomycin/penicillin. bEnd.3 cell line was purchased from ATCC (CRL-2299TM), while 293A cells were purchased from Invitrogen (R70507)

Cloning and adenovirus production.

Adenoviruses expressing various syndecan sequences were generated as previously reported [52]. Briefly, pre-synthetized blunt-end sequences corresponding to Sdc2 or DEP1 constructs (IDT, Coralville, IOWA) were sub-cloned into a pENTR/D-TOPO (Invitrogen) vector, and then transferred via LR recombination into a pAD/CMV/V5-DEST adenoviral vector (Invitrogen). Adenoviruses were generated by transfection of this plasmid into HEK 293A (Invitrogen) after PACI-linearization.

Growth factor stimulation and western blot analysis.

HUVEC or mouse ECs were seeded onto 6 cm plates in a complete medium. Confluent cells were serum-starved in Opti-MEM media (Thermo-Fisher #31985070) for 6–8 hrs and then stimulated with the indicated agent. Cells were rapidly washed twice with ice-cold PBS and lysed with 200 μL RIPA lysis buffer containing protease/ phosphatase inhibitor cocktail. Total lysates were cleared with a 16000g spin and protein concentration was determined using the BCA method. Samples were added with reducing loading buffer, boiled for 5 minutes and loaded on 4–15% gels for SDS-PAGE separation. Proteins were then transferred to PVDF Immobilon-P membranes (Millipore), blocked for 1hr in 5% fat-dry milk TBS-T (0.05% Tween) followed by 4°C overnight incubation the primary antibody. Protein

bands were visualized using HRP-conjugated secondary antibodies associated to enhanced chemiluminescence (Immobilon™ Western, Millipore). Signal from chemiluminescence reaction was recorded in a digital acquisition system (G-Box by Syngene) equipped with CCD camera. Linear range is automatically calculated by the software and is displayed as a histogram with each acquired image. Images without band saturation were used for densitometric quantification. Total intensity of each band was determined with ImageJ software [53]. Molecular weight on western blot images is reported in kilodaltons (kDa).

Gene Silencing in HUVEC.

HUVEC were seeded onto 6-well plates and transfected at 80% confluency with 2.5 ml Opti-MEM (Thermo Fisher) with indicated siRNA plus 2.5 μL Lipofectamine RNA iMAX (Thermo Fisher) for 6–8 hrs. Transfection mix was replaced with full media (EGM-2 MV) for 48 hours, then cell starved in 2% FBS for 6–8 hrs before growth factor stimulation. Following siRNA were used for knockdown experiments in HUVEC: Sdc2 (Origene #SR321721 – C, 40 nM), VEPTP (Sigma-Aldrich SASI_Hs02_00324728, 60 nM), PTP1B Sigma-Aldrich SAS1_Hs01_00230699, 60nM) DEP1 (Qiagen #SI0265877 HS_PTPRJ_6, 60 nM)

Analysis of cell surface protein level by biotinylation.

For evaluation of total surface protein level, confluent HUVEC or mouse ECs (10-cm dish) were transferred to an ice-bed, washed 3 times with cold DPBS, then treated with 5 ml of a solution cell-impermeable biotinylation reagent (EZ-Link™ Sulfo-NHS-LC-Biotin, Thermo Scientific #21335, 0.25 mg/ml in PBS with Calcium/Magnesium) for 1 hour at 4°C under gentle agitation. Cells were then placed back on ice, washed 3 times with 50 mM TRIS in DPBS (pH = 7.4) and lysed with 1.6 ml of RIPA buffer. Samples were spun at 16000g for 10 minutes and 1.3 ml of cleared lysate (~600μg) was used for pull-down with neutravidin agarose beads (Thermo Scientific #29202, 50 μl/sample) for 2 hours at 4°C under rotation. Beads were then washed 4 times with 1.5 ml of RIPA lysis buffer, resuspended in 90μl of 2X sample buffer and boiled for 7 minutes.

For surface internalization experiments, cells were transduced with indicated adenovirus (MOI~2) for 16 hours, serum-starved in Opti-MEM for 8 hours, stimulated with $VEGFA_{165}$ (100ng/ml) for the indicated times followed by surface biotinylation and neutravidin pull down as described above.

Co-Immunoprecipitation.

Confluent HUVEC (10-cm dish) were transduced for 24 hours in complete media (EGM-2 MV) with an adenovirus expressing mouse Sdc2 (V5 tag, MOI~6). Cells were split 1:3, allowed to grow for 3 more days and then transduced again with DEP1 (HA tag, MOI~2) for 24 hours. Before immune-precipitation, cells were incubated for 1.5 hours with rabbit IgG (5μg/ml) or Sdc2 pAb (5μg/ml), then washed twice with ice-cold PBS, lysed in 1.6 ml in 1% Triton lysis buffer and spun at 16000g for 10 minutes. 600μg (~1.3ml) of cleared lysate was immunoprecipitated with 50μl/sample of preabsorbed anti-V5 magnetic beads (Chromotek #v5tma, beads were preabsorbed with 1.6 ml of HUVEC cell lysate for 1hr at 4°C) for 1

hour at 4°C under gentle rotation. Magnetic beads were washed 3 times with 1.5 ml Triton lysis buffer, resuspended in 80ul of 1X sample buffer and boiled for 5 minutes.

Immunocytochemistry.

Since we were unable to obtain an effective antibody against DEP1 and Syndecan-2 (SDC2) for immunocytochemistry, we infected HUVEC for 48 hours with adenovirus expressing N-terminal HA-tagged human DEP1 to visualize DEP1 cellular localization, and N-terminal HA-tagged or SNAP-tagged human SDC2 to visualize Syndecan-2. After the indicated treatment cells were processed for immunocytochemistry. Briefly, cells were first washed with PBS, fixed in 4% PFA for 10 minutes, and permeabilized by incubation in 2% PFA, 0.1% Triton-X, 0.1% NP-40 for an additional 10 minutes. Blocking was performed by incubation in 3% BSA (in PBS) for 1 hour at room temperature. Cells were then incubated overnight at 4°C in 1% BSA (in PBS) containing appropriate primary antibodies. The following primary antibodies were used: rabbit anti-Rab5 (Cell Signaling, #3547 1:200); goat anti-VEGFR2 (R&D, #AF357, 1:100); mouse anti-HA.11 (Covance, #MMS-101P, 1:200); rabbit anti-HA (Cell signaling, #3724, 1:200); rabbit anti-VE-cadherin (Cell Signaling, #2500, 1:200); goat anti-mouse VE-cadherin (R&D Systems, #AF1002, 1:100); rat anti-mouse Flk1 (BD, #555307, 1:100). On the following day, cells were washed with PBS and incubated in 1% BSA (in PBS) containing appropriate Alexa-flour conjugated secondary antibodies used at a dilution of 1:400 for 1 hour at room temperature. Cell nuclei were counterstained with DAPI (Thermo Fisher Scientific #62248, 1:1000) for 5 minutes at room temperature. After washing in PBS, cells were mounted with glass coverslips using Prolong Gold antifade mountant (Thermo Fisher Scientific, #P36930). Imaging was performed using Leica SP8 confocal with X63 objective (Leica) or SIM microscopy as described in detail below. Colocalization analysis and quantification was obtained with Velocity 3D Image Analysis Software (PerkinElmer).

Assessment of internalized SDC2/DEP1 complex and SDC2/VEGFR2 and DEP1/VEGFR2 complex in Rab5 early endosomes.

HUVEC were plated on gelatin-coated 20 mm glass-bottom plates (Cellvis, D29–20-1.5-N). After transfection with the indicated adenovirus, cells were starved overnight in OPTImem and then placed on ice for 15 minutes to stop constitutive receptor internalization. For DEP1/SDC2 complex labeling, cells were incubated with 0.4 uM of SNAP-Surface Alexa Fluor 488 substrate (New England Biolabs, #S9129S) and a mouse anti-HA.11 (Covance, #MMS-101P, 1:200) diluted in starvation media for 30 minutes on ice and then washed with cold PBS. For DEP1 or SDC2 and VEGFR2/Rab5 complex labeling, cells were incubated with a mouse anti-HA.11 (Covance, #MMS-101P, 1:200) and an antibody against the extracellular domain of VEGFR2 (R&D, #AF357, 1:100) diluted in starvation media for 20 minutes on ice and then washed with cold PBS. Cells were then stimulated with pre-warmed media containing 50 ng/ml VEGFA165 at 37°C for 20 min to induce antibody-bound proteins internalization. After stimulation, residual antibody on the cell surface was removed by washing cells with cold acidic PBS (pH 2.5) and cells were then processed for immunocytochemistry.

For evaluation of constitutive endocytosis of DEP1 and DEP1/SDC2 complexes, HUVEC cells were first silenced for Sdc2 for 48 hours. Cells were then seeded in gelatin-coated 20 mm glass-bottom plates and infected with DEP1-HA or DEP1-HA and SDC2-SNAP adenovirus for 48 hours. After transfection cells were kept overnight in OPTImem and then labeled with the indicated antibody at room temperature for 20 minutes. Cells were then placed in incubator at 37C. At the indicated time point (0min; 15min; 30min; 1 hour), cells were washed twice with cold acidic PBS (pH 2.5) and cells were then processed for immunocytochemistry.

Assessment of internalized DEP1 and VEGFR2 in Mouse ECs.

Mouse primary cells were isolated from lung or heart of wild-type or Sdc2−/− mice. Cells were plated on fibronectin-coated 35 mm glass-bottom dishes and infected for 48 hours with 10μl of media from 293A infected with adenovirus expressing human DEP1-HA tagged protein. After overnight starvation, cells were incubated with anti-HA-tag rabbit antibody (Cell signaling, #3724, 1:100) and with an antibody against the extracellular domain of mouse VEGFR2 (Flk1) (BD, #555307, 1:100) diluted in starvation media for 15 minutes on ice and then washed with cold PBS. Cells were then stimulated with pre-warmed media containing 50 ng/ml VEGFA165 at 37°C for 20 minutes, to induce antibody-bound DEP1 and VEGFR2 internalization and trafficking. Cells were then processed for differential labeling of cell-surface and internalized proteins as described in Carrodus et al.,2014 [54]. Briefly, cells were washed twice with PBS and fixed with 4%PFA for 10 minutes. After an additional wash with PBS, cells were blocked in 5%BSA (in PBS) for 30 minutes at room temperature. To label superficial DEP1-HA expression, un-permeabilized cells were incubated for 1 hour at room temperature in 1% BSA (in PBS) containing anti-rabbit IgG Alexa Fluor-568 (Thermo Fisher Scientific, #A10042, 1:400) secondary antibody. After PBS wash, cells were incubated overnight at room temperature with an unlabeled secondary antibody raised against the species in which the primary antibody was raised. AffiniPure Fab fragment Goat anti-Rat IgG (H+L) (Jackson Immuno, #112.005.003, 0.13mg/ml) was used to block superficial anti-VEGFR2 primary antibody, while AffiniPure Fab fragment Goat anti-Rabbit IgG (H+L) (Jackson Immuno, #111.005.144, 0.13mg/ml) was used to block any superficial anti-HA primary antibody that was not fully bound by the labeled secondary antibody. The day after, cells were washed in PBS twice and post-fixed in 4%PFA for 5 minutes at room temperature. Cells were then permeabilized and blocked with 5% BSA (in PBS) containing 0.1% Triton-X-100 at room temperature for 30 min. To label internalized proteins, cells were incubated for 1 hour at room temperature in 1% BSA (in PBS) containing the following secondary antibodies: an anti-Rat IgG Alexa Fluor-647 (Thermo Fisher Scientific, #A-21472, 1:400) was used for internalized VEGFR2 labeling, and a second anti-rabbit fluorescently-conjugated secondary antibody tagged with a different fluorophore was used to label internalized DEP1-HA protein, in this case anti-rabbit IgG Alexa Fluor-488 (Thermo Fisher Scientific, #A-21206, 1:400). Cell nuclei were counterstained with DAPI (Thermo Fisher Scientific, #62248, 1:1000) for 5 minutes at room temperature. After washing in PBS, cells were mounted with glass coverslips using Prolong Gold antifade mountant (Thermo Fisher Scientific, #P36930). Imaging was performed using Leica SP8 confocal with X63 objective (Leica).

Structural Illumination microscopy (SIM).

Structural Illumination microscopy (SIM) images were acquired on the OMX version 3 system (Applied Precision) using a U-PLANAPO 60X/1.42 PSF, oil immersion objective lens (Olympus) and CoolSNAP HQ2CCD cameras with a pixel size of 0.080 mm (Photometrics). Samples were illuminated with 488, 561, and 642 nm solid-state lasers (Coherent and MPB communications) and acquired as described before [29]. Raw images were processed, reconstructed, and aligned to reveal structures with 100–125 nm resolution using Softworx software (Applied Precision). Colocalization analysis and quantification was obtained with Velocity 3D Image Analysis Software (PerkinElmer).

Vesicles Co-localization measurements.

In order to measure protein co-localization inside Rab5+ endosomes, we combined an object-based quantification method with a pixel-based method using Volocity software (Perkin-Elmer). We first segmented the images into objects and pre-processed the images to correct background noise and illumination as described in Bolte et al., 2006. Only objects with SD=2.5 as lower threshold limit and minimum object size equal to 0.1 μm^2 were selected. Objects were then filtered by 2 interactions of dilation, and excluded by size; objects with a size smaller than 0.25 μm^3 were excluded. Next, we measured the co-localization inside all the objects of the image by comparing the pixel intensities of the different channels and determining the correlation between them using the Pearson's correlation coefficient, either manually setting the threshold to 1500 AU or following automated threshold calculation based on Costes et al., 2004. For line profile measurements, we drew a line across the selected object to show an overlay displaying the intensities of each channel along that line, illustrating the distance between DEP1, Sdc2 and Rab5 or DEP1, Sdc2 and VEGFR2 inside the selected endosome.

bEnd.3 cell *in vitro* permeability, proliferation and migration.

Permeability and proliferation assays were performed with the xCELLigence RTCA System (Agilent). This allows measurement of electrical resistance of the culture plates surface over time. For permeability assay, 30000 bEnd.3 cells well were seeded onto E-Plate 16 (Agilent #5469830001) in DMEM containing 5% FBS. After ~ 60 hours, rabbit IgG (5μg/ml) or Sdc2 pAb (5μg/ml) was added to plate wells follow by $VEGFA_{165}$ stimulation (100 ng/ml). Permeability curve show changes in electrical resistance (cell index) following $VEGFA_{165}$-induced EC monolayer permeability (cell index is measured every 15minutes). For proliferation assay, 5000 bEnd.3 cells were seeded in E16 plates in DMEM containing DMEM containing 5% FBS in the presence of either rabbit IgG (5μg/ml) or Sdc2 pAb (5μg/ml) and VEGFA165 (100ng/ml). Proliferation curves show ~50 hours of monitoring (cell index is measured every 15minutes).

ECs migration was assessed using an in vitro wound healing assay as previously reported[52]. Briefly, cells were seeded on Ibidi-culture inserts (Ibidi, #80209) to create a wound between two adjacent EC monolayers. At confluency, inserts were removed, and cells allowed to migrate. Pictures of wound width were taken before and after stimulation (8 hours) and % wound closure was calculated.

Antibody generation and direct ELISA Assay.

A custom Sdc2 polyclonal antibody was generated by immunization of rabbits with a peptide corresponding to DEP1-binding motif of mouse Sdc2 (AA 124–141) and purified via affinity chromatography (GenScript USA Inc).

For direct ELISA assay, 96-well plates (Thermo Scientific #15041) were coated overnight with increasing amounts of recombinant mouse Sdc2 (R&D Systems #6585-SD-050) or mouse Sdc4 (R&D Systems 6267-SD-050). Plates were incubated with Sdc2 pAb (5μg/ml) for 1 hour at room temperature followed by secondary anti-rabbit HRP for 1 hour and chemiluminescence detection.

Assessment of vascular permeability *in vivo*.

For assessment of stimuli-induced permeability we used Miles assay (skin permeability). Briefly, anesthetized mice were injected IV with 50μl of a 2% Evans blue saline solution (sterile). After 10 minutes, vascular permeability was induced with intradermal injections of 50 μl bolus of $VEGFA_{165}$ (200ng) or histamine (Sigma-Aldrich # H7250, 100μM) on one side of shaved back skin. The opposite side was injected with PBS (control). After 30 minutes ($VEGFA_{165}$) or 15 minutes (Histamine) mice were euthanized, skin around injection sites was excised and placed in tubes with 1 ml formamide for extraction of Evans blue (55°C for 3 days). Extracted Evans blue is quantified with a spectrophotometer reader at 620 nm absorbance.

For baseline vascular permeability, mice were injected with 50μl of a 2% Evans blue saline solution (sterile) and allow to circulate for 30 minutes. Mice were euthanized, gravity-perfused with PBS (30 ml) then samples from organs collected and weighted. Samples were then placed in tubes with 1ml formamide to extract leaked Evans blue as described for Miles assay.

Cornea Pocket Assay.

Slow-releasing pellets containing $VEGFA_{165}$ were surgically implanted into the mouse cornea [55,56] and IgG or Sdc2 pAb were injected systemically after 1hr from pellet implantation. One week after pellet implantation, eyeballs were collected, corneas dissected and immunostained with anti-mouse CD31 antibody (R&D #AF3628, 1:200 dilution) to quantify neovessels formation with ImageJ (NIH).

Stroke model (permanent occlusion model)

All mouse experimental protocols have been approved by the Institutional Animal Care & Use Committee (IACUC) at Yale University. The authors have complied with all relevant animal testing and research ethical regulations.

Mice were anesthetized with ketamine/xylazine and kept on warm water re-circulating heating pad during all procedure. Mouse eyes were protected from corneal damages during a surgery using an ophthalmic lubricating ointment. Buprenorphine was given 20 minutes prior to surgery to induce preemptive analgesia. An incision was made between the left eye and ear under an operating microscope and the temporal muscle was cut and divided

exposing the left lateral aspect of the skull. Local incision was infiltrated with a local anesthetic bupivacaine. The middle cerebral artery (MCA) and branches were identified through the semi-translucent skull and a small burr hole was made using a high-speed microdrill, leaving the dura intact. Saline was applied to the area throughout the procedure to prevent heat injury, keeping the area always hydrated. Permanent focal stroke model was induced by MCA occlusion using 11–0 suture ligation. The incision was closed by two layers. After 24h from stroke onset, mice were euthanized, brain extracted, quickly sectioned with a brain matrix (1mm sections), and TTC(2,3,5-Triphenyltetrazolium chloride) live staining was performed. For mouse treatment, either rabbit IgG (100 μg/mouse) or Sdc2 pAb (100 μg/mouse) was injected I.V. 1 hour before (prevention) or 1 hour after stroke (therapy) surgery.

Stroke model (transient MCA occlusion model)

The *in vivo* protocol was approved by the Institutional Animal Care & Use Committee of Yale University. All procedures were performed following these enforced guidelines and regulations and compliance with the ARRIVE guidelines.

Pre-emptive buprenorphine was given 30 minutes before this surgical procedure. Anesthesia was induced with an intraperitoneal (IP) injection of ketamine (8.7 mg/ml) and xylazine (2 mg/ml). The body temperature was kept constant at 37.4 ± 1°C using a water-circulating heating pad. All surgical manipulations were performed under aseptic conditions. Lidocaine (2%) was injected subcutaneously before the midline incision was made in the neck. Under a Zeiss dissecting microscope, submandibular glands were bluntly dissected to expose the right common carotid artery (CCA), the proximal external carotid artery (ECA), and the proximal segment of the internal carotid artery (ICA). The distal ECA was permanently ligated with 6–0 silk. The ICA and CCA were temporarily tightened with a 6–0 silk. After an arteriotomy was performed at the proximal ECA, the 6–0 silicone rubber-coated monofilament was introduced into the ECA and advanced to occlude the middle cerebral artery (MCA) via the right ICA for 45 mins. The filament was withdrawn for the MCA reperfusion. The neck incision was closed with 6–0 prolene. Once on sternal, the animal was returned to the home cage on a heating pad until fully conscious. Sham-operated animals underwent the surgical procedure with permanent ligation of the external carotid artery and branches but without intravascular intervention with the filament. 0.1 ml antibody or vehicle was given 30 minutes after reperfusion via direct injection into the right jugular vein. 0.3 ml of saline was injected IP to prevent dehydration 2 h after ischemia/reperfusion injury.

MRI (magnetic resonance imaging) scanning

Mice were anesthetized during the MRI with ~1% isoflurane. Breathing rate was measured by placement of a respiration pad under the torso, and temperature was monitored through a rectal fiber-optic probe thermometer.

MRI data were acquired on a 11.74T horizontal-bore Bruker Avance system interfaced with Bruker ParaVision v6.0.1 software (Billerica, MA) using ^{1}H volume coil (4 cm). Shimming was done using an ellipsoid region to bring the water linewidth to less than 30 Hz using B0 mapping with second-order shim. T2 weighted anatomical MRI was first performed

using a spin-echo sequence in axial orientation (FOV: 19.2×19.2 mm3, 128×128 in-plane resolution) with TR/TE=2500/25ms with slice thickness of 1 mm. T2 mapping was based on multi echo sequence with 10 echo times TE (10 – 100 ms) with TR = 4000 ms) with the same FOV and in plane resolution as T2 weighted anatomical MRI. The multiple echo times enabled voxel-wise calculations of T2 values. Voxel-wise T2 maps were calculated by fitting MRI voxel intensities versus the series of TE values to a monoexponential curve e-TE/T2. Diffusion weighted (spin echo planar (SE-EPI)) imaging was performed with TR/TE=4000/26.18 ms, FOV: 19.2×19.2 mm3, 128×128 in-plane resolution, slice thickness 1mm, to assess ischemically injured tissue and edema. WE used 3 directions and 6 b values (0, 50, 100, 250, 500, 1000 s/mm2) with voxel-wise calculated quantitative apparent diffusion coefficient (ADC) maps.

Noninvasive quantitative cerebral blood flow (CBF) was carried out to identify the perfusion deficit on 1mm thick slices throughout the MCAO region using a form of pseudo-continuous arterial spin labeling (ASL), flow-alternating inversion recovery (FAIR) MRI. The sequence employs a spin echo EPI imaging module (TR/TE=10000/14ms, FOV=32×32 mm3, 85×85 matrix size, 1mm slice thickness with 1mm gap). Voxel-based analysis generated using codes written in Matlab (MathWorks, Natick, MA, USA) allowed unbiased analysis of the spatial, volumetric, and dynamic evaluation of different tissue compartments. Tissue was compartmentalized using in-house defined thresholds set for two parameters: 1) T2 and R2 (1/T2) signal change and ADC and 2) ADC and CBF dataset for diffusion/perfusion mismatch. Color coded images were created enabling analysis of changes in voxel distribution across ischemic core, penumbra/edema and nonischemic tissue. Lesion and hemispheric volumes were determined on T2-weighted images. The hemispheres were traced manually on each slice. The position of the midline was determined with the use of the following neuroanatomic landmarks: falx cerebri, corpus pineale, fissura longitudinalis, infundibulum, aqueductus cerebri, and third ventricle as described by Gerriets [57]. Lesion volumes were determined from ADC maps by tracing of the hypointense lesions. The areas were then summed and multiplied by the slice thickness. Lesion volumes were calculated with and without edema correction and expressed as percentage of the hemispheric volume [57].

Data availability Statement

All data supporting the findings of this study are available within the paper and associated files. Source data are provided with this paper.

Extended Data

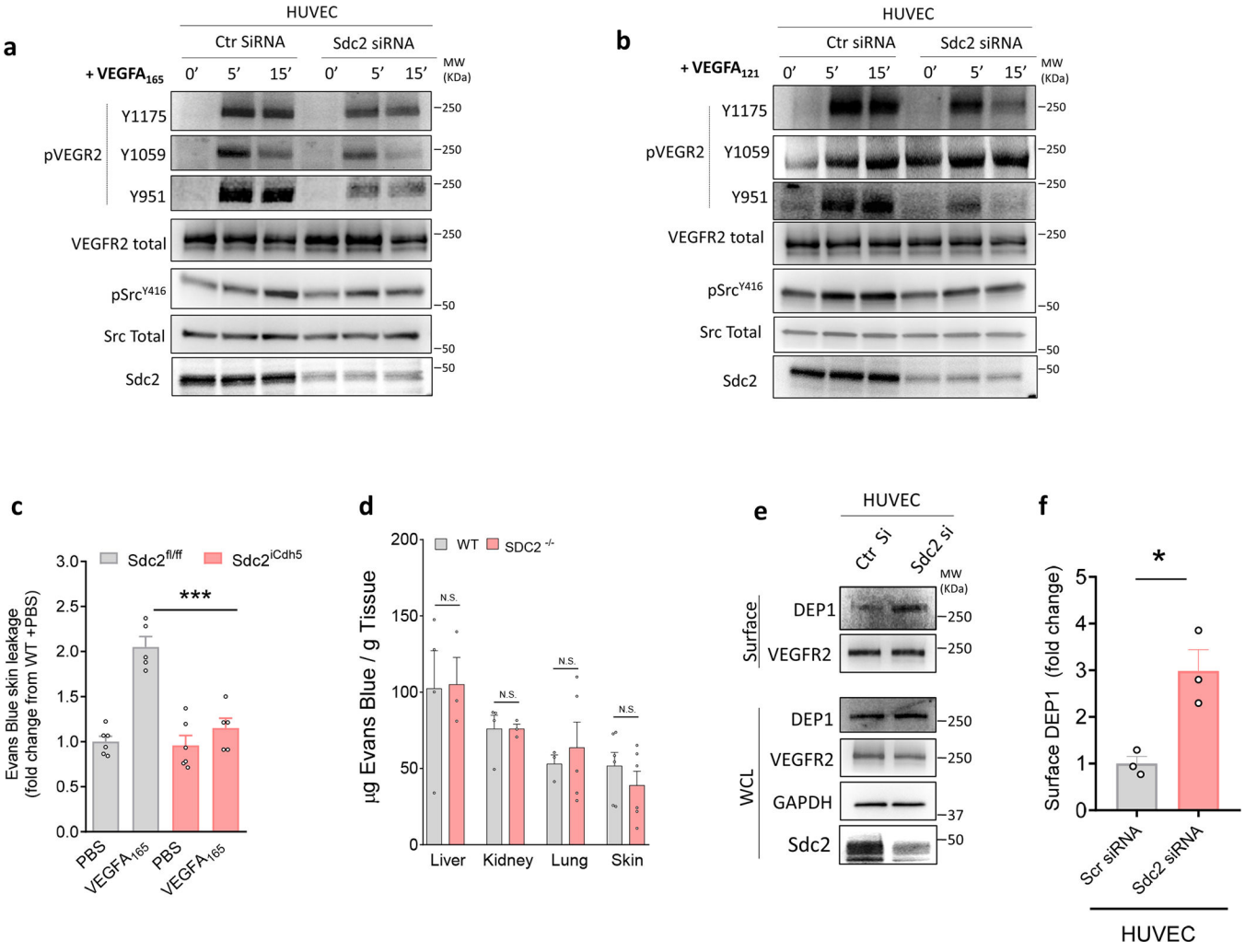

Extended Data Fig. 1.

a-b, western blot analysis of VEGFR2 phosphorylation (pVEGFR2) following stimulation with VEGFA165 (50ng/ml) or VEGFA121 (50ng/ml) in Control (Ctr Si) vs. Sdc2-depleted (Sdc2 siRNA) HUVEC. **c**, VEGFA165 -induced Evans blue leakage in the back skin of WT vs Sdc2iECKO mice (n=5–6) (representative blots of 3 independent experiments). **d**, evaluation of baseline permeability in various organs measured as Evans blue dye leakage in Wild type (WT) vs Sdc2−/− mice (n=3–6). **e, f** western blot analysis of cell surface protein levels in Control (Ctr) vs. Sdc2-depleted (Sdc2 siRNA) HUVEC (n=3). Data are presented as mean values +/− SEM (standard error of the mean). In all figure panels, each dot represents a biological independent experiment (n). Statistical analysis was performed by one-way ANOVA with Sidak's multiple comparison test (panels c, d), and by unpaired t-student test (panel f), (N.S. not significant, * P<0.05, ** P <0.01, *** P<0.001).

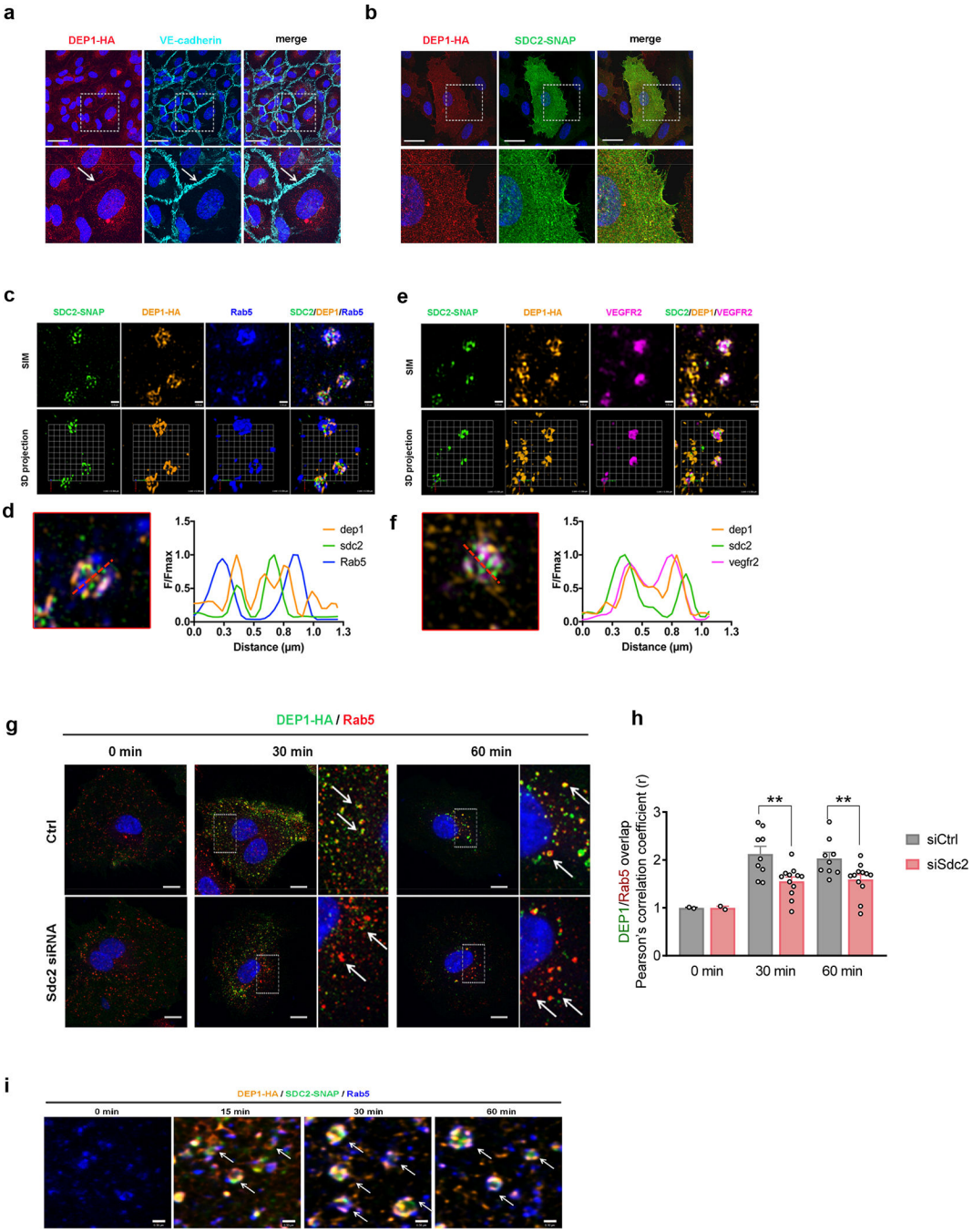

Extended Data Fig. 2.

a, confocal image of confluent HUVEC cells in basal conditions showing human DEP1 carrying N-terminal HA-tag (DEP1-HA, red) expression at cell-cell junctions labeled with VE-cadherin (cyan), white arrows, lower panels. Scale bar: 25 µm. **b**, confocal image of HUVEC cells in basal conditions expressing both human DEP1 carrying N-terminal HA-tag (DEP1-HA, red) and human Sdc2 carrying N-terminal SNAP-tag (SDC2-SNAP, green) proteins. Lower panels show magnification of box in upper panels showing localization of both proteins at the plasma membrane and at the membrane protrusions. Scale bar:

25 μm. **c, f**, SIM imaging of SDC2/DEP1/Rab5 and SDC2/DEP1/VEGFR2 complexes in HUVECs expressing DEP1-HA and SDC2-SNAP proteins and treated for 20 minutes with 50ng/ml VEGFA165. Scale bar: 0.5 μm. **d,f**, line profile analysis illustrating the distance between DEP1, Sdc2 and Rab5 or DEP1, Sdc2 and VEGFR2 in the same compartment. Plots represent the fluorescent signal in SIM images as a function of position along the line profile in left panel (red dotted line). **g, h** confocal images of constitutive internalization of DEP1 after incubation for 0 min, 30 min and 60 min in absence of VEGFA in HUVECs control and HUVECs transfected with Sdc2 siRNA. Scale bar: 15 μm. **i**, confocal image of internalized SDC2-DEP1 complexes in Rab5+ endosomes (white arrows) following constitutive endocytosis in VEGFA-free media. Scale bar: 5 μm.

All images are representative images of >3 independent experiments (n).

Data are presented as mean values +/− SEM (standard error of the mean). Statistical analysis was performed by two-way ANOVA with Sidak's multiple comparison test (panels h), (N.S. not significant, * P<0.05, ** P <0.01, *** P<0.001).

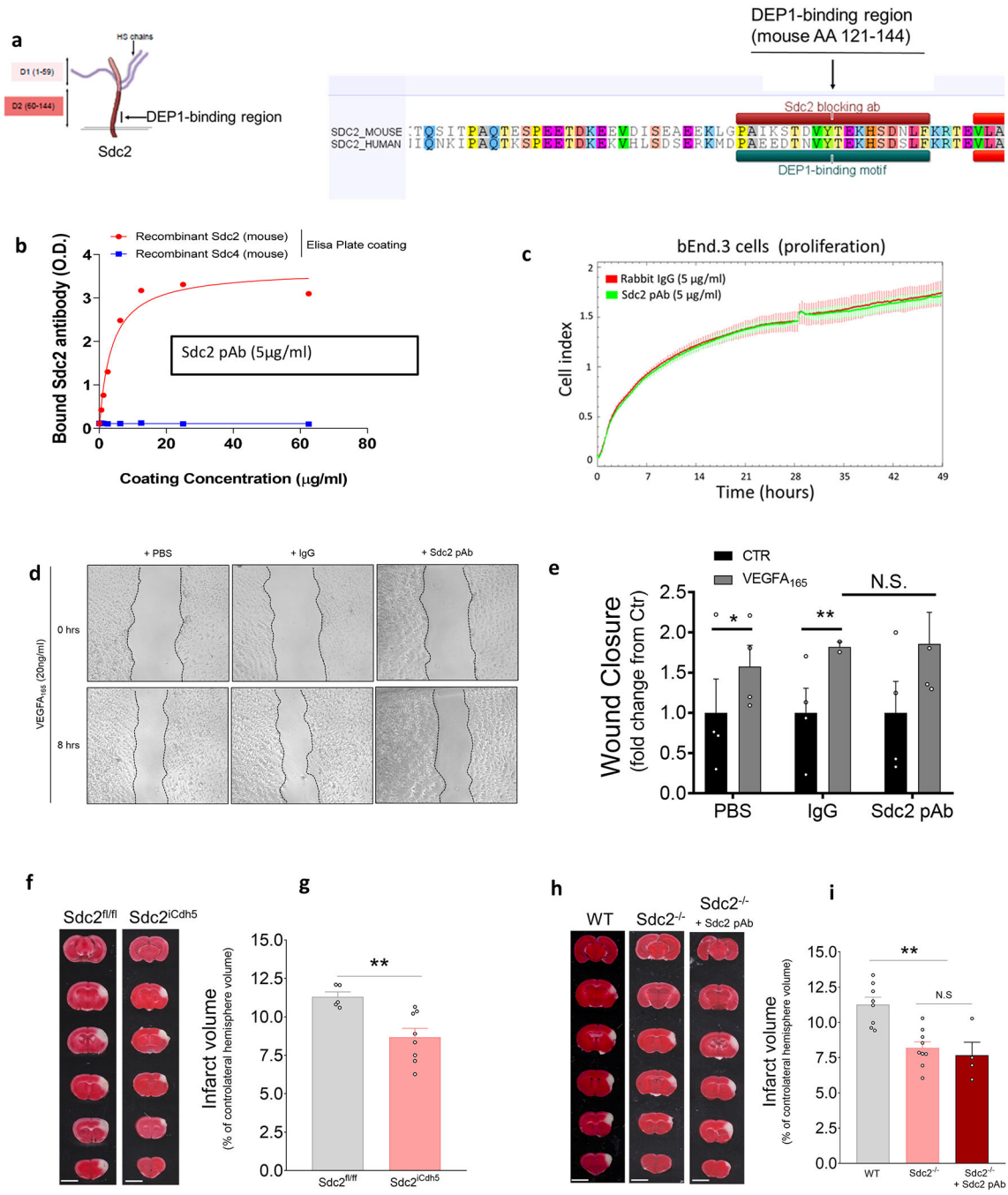

Extended Data Fig. 3.

a, position and sequence of DEP1-binding motif in human Sdc2. **b**, direct ELISA comparing Sdc2 pAb (5µg/ml) binding to mouse Sdc2 vs. mouse Sdc4. **c**, bEnd.3 cell proliferation in presence of rabbit IgG (5µg/ml) or Sdc2 pAb (5µg/ml) measured with xCELLigence system. **d-e**, ECs migration measured by in vitro wound healing assay in bEnd.3 cells in presence of rabbit IgG (5µg/ml) or Sdc2 pAb (5µg/ml) (n=3–4) **f-g**, TTC staining (at 24 hours post stroke) and quantification of stroke infarct in WT vs Sdc2iECKO (n=5–8). **h-i**, TTC staining

(at 24 hours post stroke) in Sdc2−/− mice with or without Sdc2 pAb treatment (administered 1 hour before stroke) (n=4–9).

Data are presented as mean values +/− SEM (standard error of the mean). In all figure panels, each dot represents a biological independent experiment (n). Statistical analysis was performed by one-way ANOVA with Sidak's multiple comparison test (panels e, i), and by unpaired t-student test (panel g), (N.S. not significant, * P<0.05, ** P <0.01, *** P<0.001).

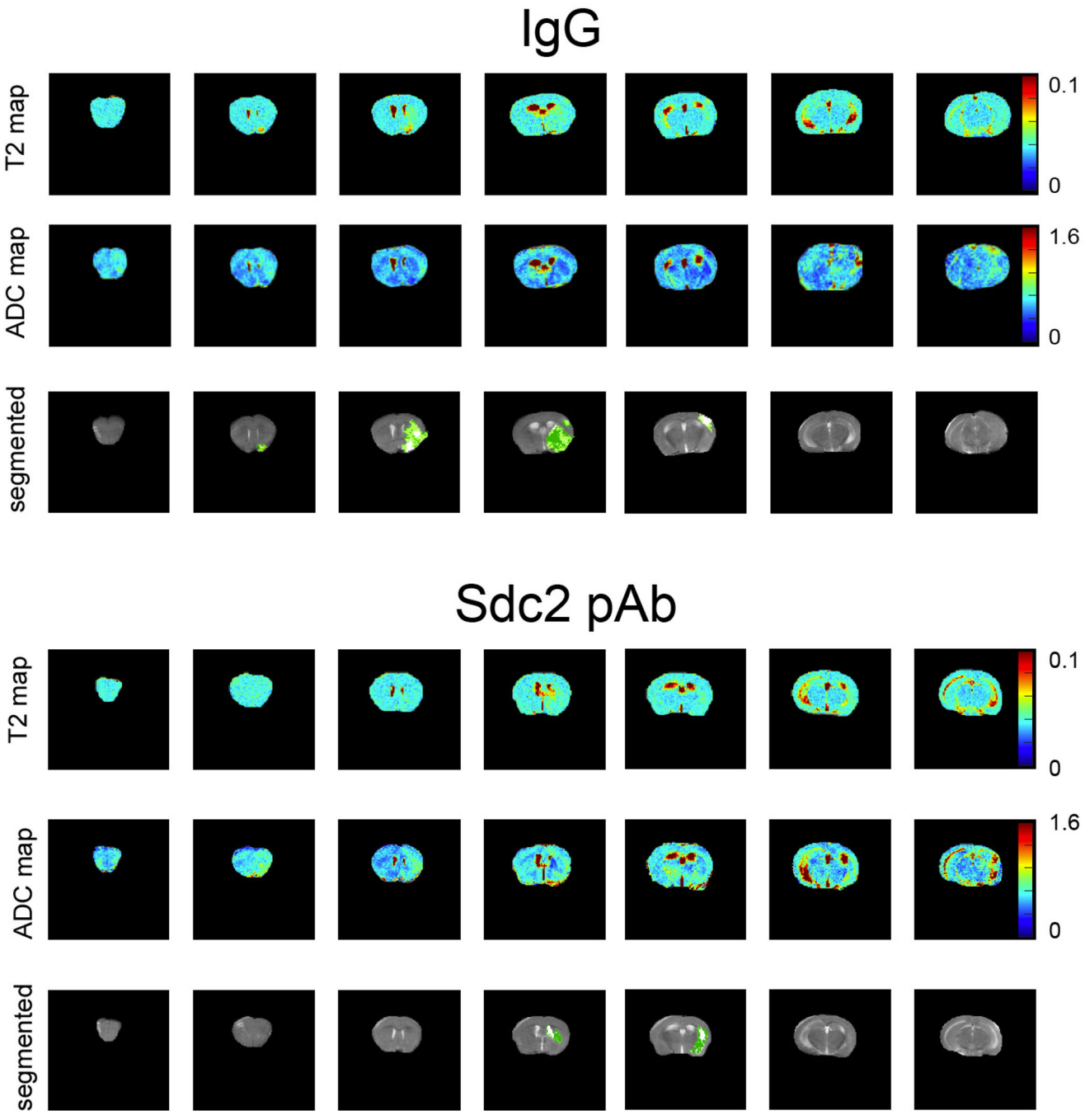

Extended Data Fig. 4.

MR imaging of IgG and Sdc2 pAb treated mice: Representative T2 maps from mouse treated with IgG and Sdc2 pAb showing relatively well defined heterogeneous, hyperintense area within right MCA territory with measured T2 values in a range of 0.05–0.09 ms which were higher compared with contralateral normal tissue average 0.03 ms. On the ADC map, in the same region there is hypointense area with low ADC values, range from 0.4–0.8×10–3mm2/s, due to restricted diffusion. In normal appearing contralateral tissue measured ADC values were 0.9–1.1×10–3mm2/s. Compartmentalization analysis (see Material and Methods for details) shows different compartments of ischemic stroke; core (white), penumbra (light green) and edema (dark green).

Supplementary Material

Refer to Web version on PubMed Central for supplementary material.

Acknowledgments

We thank Dongying Chen for the technical assistance and helpfull discussion regarding the corneal pocket assay and confocal imaging

References

1. Bates DO Vascular endothelial growth factors and vascular permeability. Cardiovasc Res 87, 262–271, doi:10.1093/cvr/cvq105 (2010). [PubMed: 20400620]
2. Park-Windhol C & D'Amore PA Disorders of Vascular Permeability. Annu Rev Pathol 11, 251–281, doi:10.1146/annurev-pathol-012615-044506 (2016). [PubMed: 26907525]
3. Claesson-Welsh L, Dejana E & McDonald DM Permeability of the Endothelial Barrier: Identifying and Reconciling Controversies. Trends Mol Med 27, 314–331, doi:10.1016/j.molmed.2020.11.006 (2021). [PubMed: 33309601]
4. van Bruggen N et al. VEGF antagonism reduces edema formation and tissue damage after ischemia/reperfusion injury in the mouse brain. J Clin Invest 104, 1613–1620, doi:10.1172/JCI8218 (1999). [PubMed: 10587525]
5. Croll SD et al. VEGF-mediated inflammation precedes angiogenesis in adult brain. Exp Neurol 187, 388–402, doi:10.1016/j.expneurol.2004.02.010 (2004). [PubMed: 15144865]
6. Barratt S, Medford AR & Millar AB Vascular endothelial growth factor in acute lung injury and acute respiratory distress syndrome. Respiration 87, 329–342, doi:10.1159/000356034 (2014). [PubMed: 24356493]
7. Sharp C, Millar AB & Medford AR Advances in understanding of the pathogenesis of acute respiratory distress syndrome. Respiration 89, 420–434, doi:10.1159/000381102 (2015). [PubMed: 25925331]
8. Orsenigo F et al. Phosphorylation of VE-cadherin is modulated by haemodynamic forces and contributes to the regulation of vascular permeability in vivo. Nat Commun 3, 1208, doi:10.1038/ncomms2199 (2012). [PubMed: 23169049]
9. Sun Z et al. VEGFR2 induces c-Src signaling and vascular permeability in vivo via the adaptor protein TSAd. The Journal of experimental medicine 209, 1363–1377, doi:10.1084/jem.20111343 (2012). [PubMed: 22689825]
10. Simons M, Gordon E & Claesson-Welsh L Mechanisms and regulation of endothelial VEGF receptor signalling. Nature reviews 17, 611–625, doi:10.1038/nrm.2016.87 (2016).
11. Smith RO et al. Vascular permeability in retinopathy is regulated by VEGFR2 Y949 signaling to VE-cadherin. Elife 9, doi:10.7554/eLife.54056 (2020).
12. Eliceiri BP et al. Selective requirement for Src kinases during VEGF-induced angiogenesis and vascular permeability. Molecular cell 4, 915–924 (1999). [PubMed: 10635317]

13. Paul R et al. Src deficiency or blockade of Src activity in mice provides cerebral protection following stroke. Nat Med 7, 222–227, doi:10.1038/84675 (2001). [PubMed: 11175854]
14. Gavard J & Gutkind JS VEGF controls endothelial-cell permeability by promoting the beta-arrestin-dependent endocytosis of VE-cadherin. Nat Cell Biol 8, 1223–1234, doi:10.1038/ncb1486 (2006). [PubMed: 17060906]
15. Elias BC et al. Phosphorylation of Tyr-398 and Tyr-402 in occludin prevents its interaction with ZO-1 and destabilizes its assembly at the tight junctions. The Journal of biological chemistry 284, 1559–1569, doi:10.1074/jbc.M804783200 (2009). [PubMed: 19017651]
16. Fantin A et al. VEGF165-induced vascular permeability requires NRP1 for ABL-mediated SRC family kinase activation. The Journal of experimental medicine 214, 1049–1064, doi:10.1084/jem.20160311 (2017). [PubMed: 28289053]
17. Gitay-Goren H, Soker S, Vlodavsky I & Neufeld G The binding of vascular endothelial growth factor to its receptors is dependent on cell surface-associated heparin-like molecules. The Journal of biological chemistry 267, 6093–6098 (1992). [PubMed: 1556117]
18. Chiodelli P, Bugatti A, Urbinati C & Rusnati M Heparin/Heparan sulfate proteoglycans glycomic interactome in angiogenesis: biological implications and therapeutical use. Molecules 20, 6342–6388, doi:10.3390/molecules20046342 (2015). [PubMed: 25867824]
19. Corti F et al. N-terminal syndecan-2 domain selectively enhances 6-O heparan sulfate chains sulfation and promotes VEGFA165-dependent neovascularization. Nat Commun 10, 1562, doi:10.1038/s41467-019-09605-z (2019). [PubMed: 30952866]
20. Ferrara N Binding to the extracellular matrix and proteolytic processing: two key mechanisms regulating vascular endothelial growth factor action. Mol Biol Cell 21, 687–690, doi:10.1091/mbc.E09-07-0590 (2010). [PubMed: 20185770]
21. Li X et al. VEGFR2 pY949 signalling regulates adherens junction integrity and metastatic spread. Nat Commun 7, 11017, doi:10.1038/ncomms11017 (2016). [PubMed: 27005951]
22. Brash JT, Ruhrberg C & Fantin A Evaluating Vascular Hyperpermeability-inducing Agents in the Skin with the Miles Assay. J Vis Exp, doi:10.3791/57524 (2018).
23. Wang Y et al. Ephrin-B2 controls VEGF-induced angiogenesis and lymphangiogenesis. Nature 465, 483–486, doi:10.1038/nature09002 (2010). [PubMed: 20445537]
24. Hayashi M et al. VE-PTP regulates VEGFR2 activity in stalk cells to establish endothelial cell polarity and lumen formation. Nat Commun 4, 1672, doi:10.1038/ncomms2683 (2013). [PubMed: 23575676]
25. Grazia Lampugnani M et al. Contact inhibition of VEGF-induced proliferation requires vascular endothelial cadherin, beta-catenin, and the phosphatase DEP-1/CD148. The Journal of cell biology 161, 793–804, doi:10.1083/jcb.200209019 (2003). [PubMed: 12771128]
26. Fournier P et al. The protein tyrosine phosphatase PTPRJ/DEP-1 contributes to the regulation of the Notch-signaling pathway and sprouting angiogenesis. Angiogenesis 23, 145–157, doi:10.1007/s10456-019-09683-z (2020). [PubMed: 31598898]
27. Lanahan AA et al. PTP1b is a physiologic regulator of vascular endothelial growth factor signaling in endothelial cells. Circulation 130, 902–909, doi:10.1161/CIRCULATIONAHA.114.009683 (2014). [PubMed: 24982127]
28. Corti F & Simons M Modulation of VEGF receptor 2 signaling by protein phosphatases. Pharmacol Res 115, 107–123, doi:10.1016/j.phrs.2016.11.022 (2017). [PubMed: 27888154]
29. Lanahan AA et al. VEGF receptor 2 endocytic trafficking regulates arterial morphogenesis. Developmental cell 18, 713–724, doi:10.1016/j.devcel.2010.02.016 (2010). [PubMed: 20434959]
30. Ostman A, Yang Q & Tonks NK Expression of DEP-1, a receptor-like protein-tyrosine-phosphatase, is enhanced with increasing cell density. Proc Natl Acad Sci U S A 91, 9680–9684, doi:10.1073/pnas.91.21.9680 (1994). [PubMed: 7937872]
31. Takahashi T et al. Endothelial localization of receptor tyrosine phosphatase, ECRTP/DEP-1, in developing and mature renal vasculature. J Am Soc Nephrol 10, 2135–2145, doi:10.1681/ASN.V10102135 (1999). [PubMed: 10505690]
32. Adam AP Regulation of Endothelial Adherens Junctions by Tyrosine Phosphorylation. Mediators Inflamm 2015, 272858, doi:10.1155/2015/272858 (2015). [PubMed: 26556953]

33. Whiteford JR et al. Syndecan-2 is a novel ligand for the protein tyrosine phosphatase receptor CD148. Mol Biol Cell 22, 3609–3624, doi:10.1091/mbc.E11-02-0099 (2011). [PubMed: 21813734]
34. Kofler N et al. The Rab-effector protein RABEP2 regulates endosomal trafficking to mediate vascular endothelial growth factor receptor-2 (VEGFR2)-dependent signaling. The Journal of biological chemistry 293, 4805–4817, doi:10.1074/jbc.M117.812172 (2018). [PubMed: 29425100]
35. Srinivasan B & Kolli AR in Blood-Brain Barrier 99–114 (Springer, 2019).
36. Lange C, Storkebaum E, de Almodovar CR, Dewerchin M & Carmeliet P Vascular endothelial growth factor: a neurovascular target in neurological diseases. Nat Rev Neurol 12, 439–454, doi:10.1038/nrneurol.2016.88 (2016). [PubMed: 27364743]
37. Apte RS, Chen DS & Ferrara N VEGF in Signaling and Disease: Beyond Discovery and Development. Cell 176, 1248–1264, doi:10.1016/j.cell.2019.01.021 (2019). [PubMed: 30849371]
38. Simard JM, Kent TA, Chen M, Tarasov KV & Gerzanich V Brain oedema in focal ischaemia: molecular pathophysiology and theoretical implications. Lancet neurology 6, 258–268, doi:10.1016/S1474-4422(07)70055-8 (2007). [PubMed: 17303532]
39. Ma Y, Zechariah A, Qu Y & Hermann DM Effects of vascular endothelial growth factor in ischemic stroke. Journal of Neuroscience Research 90, 1873–1882, doi:10.1002/jnr.23088 (2012). [PubMed: 22714747]
40. Geiseler SJ & Morland C The Janus Face of VEGF in Stroke. Int J Mol Sci 19, doi:10.3390/ijms19051362 (2018).
41. Doyle KP & Buckwalter MS A mouse model of permanent focal ischemia: distal middle cerebral artery occlusion. Methods Mol Biol 1135, 103–110, doi:10.1007/978-1-4939-0320-7_9 (2014). [PubMed: 24510858]
42. Jin ZG et al. Ligand-independent activation of vascular endothelial growth factor receptor 2 by fluid shear stress regulates activation of endothelial nitric oxide synthase. Circ Res 93, 354–363, doi:10.1161/01.RES.0000089257.94002.96 (2003). [PubMed: 12893742]
43. Warren CM, Ziyad S, Briot A, Der A & Iruela-Arispe ML A ligand-independent VEGFR2 signaling pathway limits angiogenic responses in diabetes. Sci Signal 7, ra1, doi:10.1126/scisignal.2004235 (2014). [PubMed: 24399295]
44. Couchman JR, Gopal S, Lim HC, Norgaard S & Multhaupt HA Fell-Muir Lecture: Syndecans: from peripheral coreceptors to mainstream regulators of cell behaviour. Int J Exp Pathol 96, 1–10, doi:10.1111/iep.12112 (2015). [PubMed: 25546317]
45. De Rossi G et al. Pathological Angiogenesis Requires Syndecan-4 for Efficient VEGFA-Induced VE-Cadherin Internalization. Arteriosclerosis, thrombosis, and vascular biology 41, 1374–1389, doi:10.1161/ATVBAHA.121.315941 (2021). [PubMed: 33596666]
46. Dews IC & Mackenzie KR Transmembrane domains of the syndecan family of growth factor coreceptors display a hierarchy of homotypic and heterotypic interactions. Proc Natl Acad Sci U S A 104, 20782–20787, doi:10.1073/pnas.0708909105 (2007). [PubMed: 18093920]
47. Ruiz XD et al. Syndecan-2 is a novel target of insulin-like growth factor binding protein-3 and is over-expressed in fibrosis. PLoS One 7, e43049, doi:10.1371/journal.pone.0043049 (2012). [PubMed: 22900087]
48. Choi S et al. Inflammatory hypoxia induces syndecan-2 expression through IL-1beta-mediated FOXO3a activation in colonic epithelia. FASEB J 31, 1516–1530, doi:10.1096/fj.201601098R (2017). [PubMed: 28031321]
49. Hong H et al. Up-regulation of syndecan-2 in proximal colon correlates with acute inflammation. FASEB J 33, 11381–11395, doi:10.1096/fj.201900561R (2019). [PubMed: 31311305]
50. Zhang ZG et al. VEGF enhances angiogenesis and promotes blood-brain barrier leakage in the ischemic brain. J Clin Invest 106, 829–838, doi:10.1172/JCI9369 (2000). [PubMed: 11018070]
51. Reeson P et al. Delayed inhibition of VEGF signaling after stroke attenuates blood-brain barrier breakdown and improves functional recovery in a comorbidity-dependent manner. J Neurosci 35, 5128–5143, doi:10.1523/JNEUROSCI.2810-14.2015 (2015). [PubMed: 25834040]
52. Corti F, Finetti F, Ziche M & Simons M The Syndecan-4/Protein Kinase C alpha Pathway Mediates Prostaglandin E-2-induced Extracellular Regulated Kinase (ERK) Activation in

Endothelial Cells and Angiogenesis in Vivo. Journal of Biological Chemistry 288, 12712–12721, doi:10.1074/jbc.M113.452383 (2013). [PubMed: 23525101]

53. Schneider CA, Rasband WS & Eliceiri KW NIH Image to ImageJ: 25 years of image analysis. Nature methods 9, 671–675 (2012). [PubMed: 22930834]
54. Carrodus NL, Teng KS, Munro KM, Kennedy MJ & Gunnersen JM Differential labeling of cell-surface and internalized proteins after antibody feeding of live cultured neurons. J Vis Exp, e51139, doi:10.3791/51139 (2014). [PubMed: 24561550]
55. Tang Z et al. A mouse model of the cornea pocket assay for angiogenesis study. J Vis Exp, doi:10.3791/3077 (2011).
56. Ziche M & Morbidelli L The corneal pocket assay. Methods Mol Biol 1214, 15–28, doi:10.1007/978-1-4939-1462-3_2 (2015). [PubMed: 25468596]
57. Gerriets T et al. Noninvasive quantification of brain edema and the space-occupying effect in rat stroke models using magnetic resonance imaging. Stroke 35, 566–571, doi:10.1161/01.STR.0000113692.38574.57 (2004). [PubMed: 14739415]
58. Kovalenko M et al. Site-selective dephosphorylation of the platelet-derived growth factor beta-receptor by the receptor-like protein-tyrosine phosphatase DEP-1. The Journal of biological chemistry 275, 16219–16226, doi:10.1074/jbc.275.21.16219 (2000). [PubMed: 10821867]
59. Persson C, Engstrom U, Mowbray SL & Ostman A Primary sequence determinants responsible for site-selective dephosphorylation of the PDGF beta-receptor by the receptor-like protein tyrosine phosphatase DEP-1. FEBS Lett 517, 27–31, doi:10.1016/s0014-5793(02)02570-x (2002). [PubMed: 12062403]
60. Tarcic G et al. An unbiased screen identifies DEP-1 tumor suppressor as a phosphatase controlling EGFR endocytosis. Curr Biol 19, 1788–1798, doi:10.1016/j.cub.2009.09.048 (2009). [PubMed: 19836242]

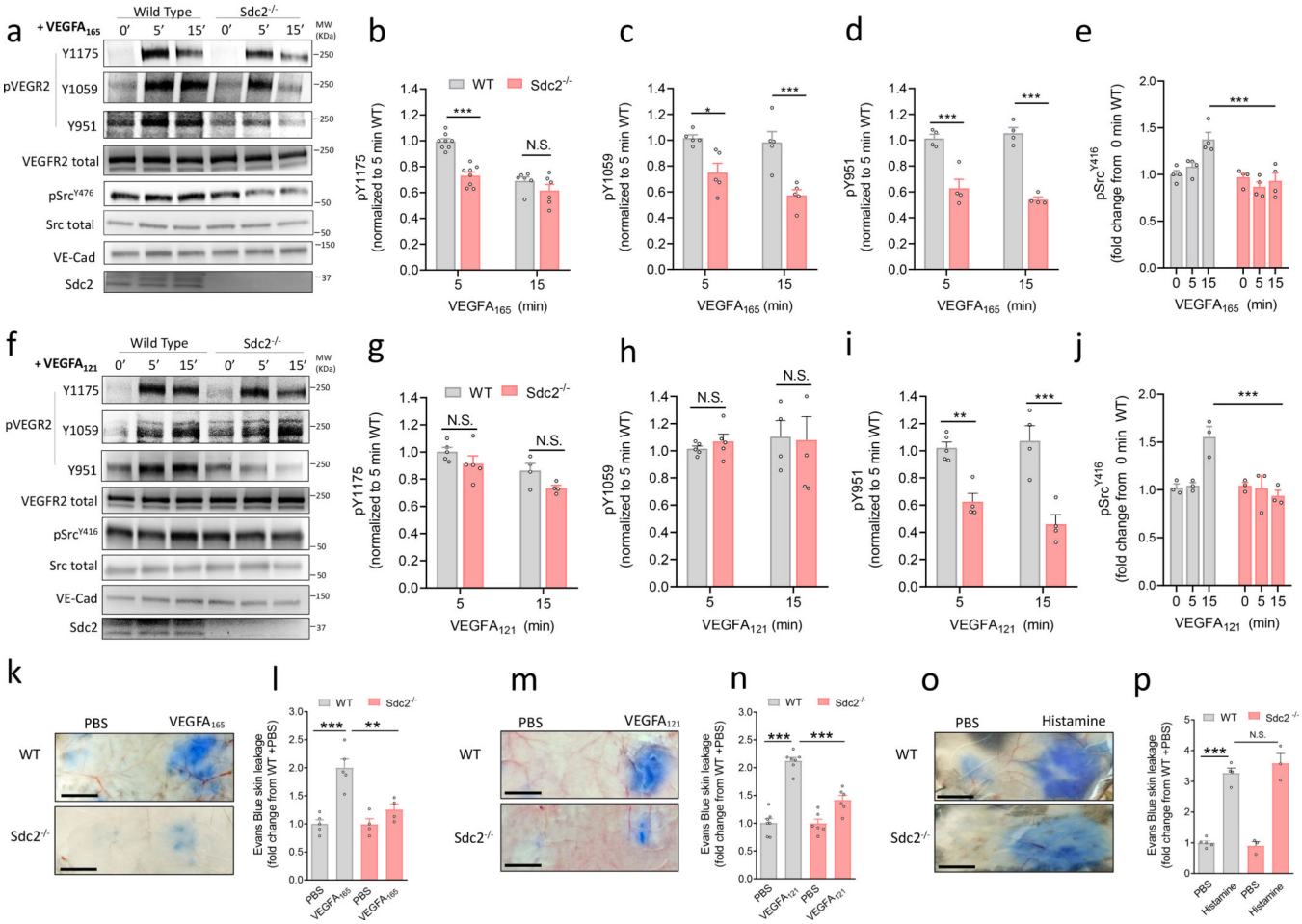

Fig. 1: Sdc2 deletion leads to reduced VEGFA-induced Y951 phosphorylation and permeability *in vivo*.

a-e, western blot analysis and quantification of VEGFR2 phosphorylation (pVEGFR2) and Src activation ($pSrc^{Y416}$) in Wild type (WT) vs $Sdc2^{-/-}$ mouse ECs after 5–15 minutes (min) of stimulation with $VEGFA_{165}$ (50ng/ml) vs PBS (phosphate-buffered saline) vehicle (n= 4–8). **f-j,** western blot analysis and quantification of VEGFR2 phosphorylation and Src activation ($pSrc^{Y416}$) in Wild type (WT) vs $Sdc2^{-/-}$ mouse ECs 5–15 minutes (min) of stimulation with $VEGFA_{121}$ (50ng/ml (n= 4–5). **k-l,** $VEGFA_{165}$ -induced Evans blue dye leakage in the back skin (Miles assay) of WT vs $Sdc2^{-/-}$ mice (Scale bars = 500μm) (n=4–5). **m-n,** $VEGFA_{121}$ -induced Evans blue dye leakage in the back skin of WT vs $Sdc2^{-/-}$ mice (Scale bars = 500μm) (n=6–7). **o-p,** histamine-induced Evans blue dye leakage in the back skin of WT vs $Sdc2^{-/-}$ mice (Scale bars = 500μm) (n=3–5).

Data are presented as mean values +/− SEM (standard error of the mean) and each dot represents a biological independent experiment (n). Statistical analysis was performed by two-way ANOVA with Sidak's multiple comparison test (panels b-e, g-j) and by one-way ANOVA with Sidak's multiple comparison test (panels l, n, p), (N.S. not significant, * P<0.05, ** P<0.01, *** P<0.001).

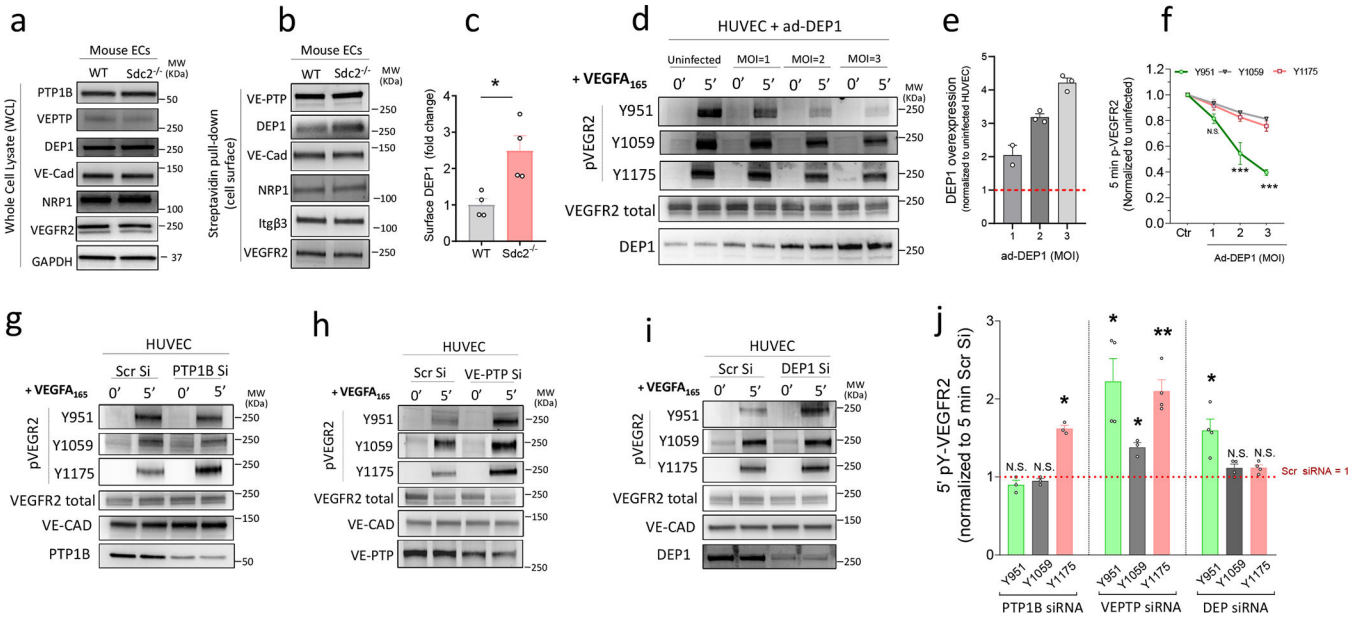

Fig. 2: Increased DEP1 surface level in Sdc2$^{-/-}$ mouse ECs promotes selective dephosphorylation of VEGFR2 Y951 (Y951 in mouse)

a, western blot analysis of protein levels in whole cell lysates (WCL) of WT vs Sdc2$^{-/-}$ mouse ECs (representative blot of 3 independent experiments). **b**, western blot analysis of cell membrane protein levels by streptavidin pull-down (cell surface) in WT vs Sdc2$^{-/-}$ mouse ECs. **c,** quantification of DEP1 level at the cytoplasmic membrane (surface) (n=4). **d-f,** assessment of VEGFA$_{165}$ -induced VEGFR2 phosphorylation (pVEGFR2) after DEP1 overexpression in HUVEC (n=3–4). Red line (panel e) represents endogenous DEP1 level normalized to 1. **g-j,** assessment of VEGFA$_{165}$ -induced VEGFR2 phosphorylation after silencing of PTP1B (PTP1B Si), VEPTP (VEPTP Si) and DEP1 (DEP1 Si) in HUVEC (n=3–4).

Data are presented as mean values +/− SEM (standard error of the mean). In all figure panels, each dot represents a biological independent experiment (n). Statistical analysis was performed by unpaired two-tailed t-student test (panel c), two-way ANOVA with Sidak's multiple comparison test (panels e, f, j), (N.S. not significant, * P<0.05, ** P <0.01, *** P<0.001).

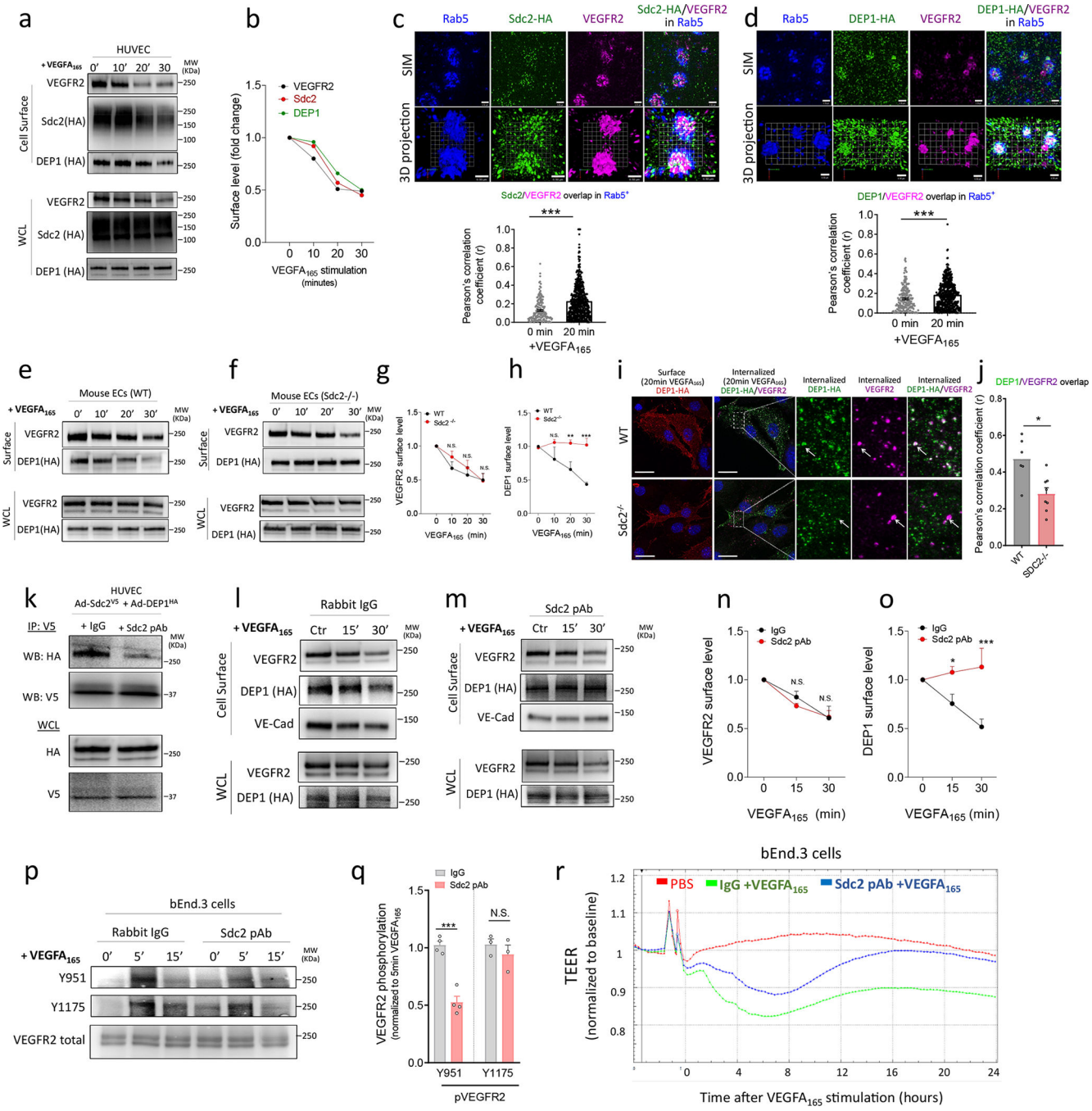

Fig. 3: Sdc2-DEP1 interaction regulates DEP1 surface level and can be exploited to achieve specific inhibition of VEGFA-induced permeability

a-b, western blot analysis and quantification of cell surface protein levels after $VEGFA_{165}$ (100 ng/ml) stimulation in HUVEC. For increased sensitivity, the experiment was performed in HUVEC after overexpression of either Sdc2 or DEP1 carrying N-terminal HA-tag. **c-d**, SIM imaging of endosomal SDC2/VEGFR2 and DEP1/VEGFR2 complexes in HUVEC expressing human Sdc2 or DEP1 carrying N-terminal HA-tag (SDC2-HA and DEP1-HA) and treated for 20 minutes with 50ng/ml VEGF. Scale bars: 0.5 μm. Quantification shows

the levels of co-localization of SDC2 or DEP1 and VEGFR2 in Rab5+ objects. Each point indicates a Rab5+ endosome. **e-h,** western blot analysis and quantification of cell surface protein levels following $VEGFA_{165}$ (100 ng/ml) in WT vs $Sdc2^{-/-}$ mouse ECs. (n=3=5). **i,** confocal imaging of primary mouse WT and Sdc2−/− ECs infected with adenovirus expressing human DEP1 carrying N-terminal HA-tag (DEP1-HA) protein and treated for 20 minutes with 50ng/ml VEGFA165. In red, the superficial expression of DEP1 shows comparable infection levels of WT and Sdc2−/− sample. The co-localization of internalized DEP1-HA (green) and internalized VEGFR2 (purple) was reduced in $Sdc2^{-/-}$ samples (white arrows). Scale bar: 25 μm **k,** Sdc2/DEP1 Co-Ip in presence of rabbit IgG (+IgG) or an antibody against DEP-binding motif in Sdc2 (Sdc2 pAb) (representative blot of 3 independent experiments).

l-o, western blot analysis of cell surface protein levels following $VEGFA_{165}$ (100 ng/ml) stimulation in bEnd.3 cells. Cells were preincubated for 1 hour with a rabbit IgG (5μg/ml) or the Sdc2 pAb (5μg/ml) before $VEGFA_{165}$ stimulation (n=3=4).

p-q, assessment of VEGFA-induced VEGFR2 phosphorylation after preincubation (1.5 hours) with a rabbit IgG (5μg/ml) or Sdc2 pAb (5μg/ml). **r,** *in vitro* permeability response in bEnd.3 cells in response to $VEGFA_{165}$ (100ng/ml) in the presence of a rabbit IgG (5μg/ml) or Sdc2 pAb (5μg/ml) (n=3–4).

Data are presented as mean values +/− SEM (standard error of the mean). In all figure panels, each dot represents a biological independent experiment (n). Statistical analysis was performed by two-way ANOVA with Sidak's multiple comparison test (panela g-h, n-o) and by one-way ANOVA with Sidak's multiple comparison (panel q) (N.S. not significant, * P<0.05, ** P<0.01, *** P<0.001).

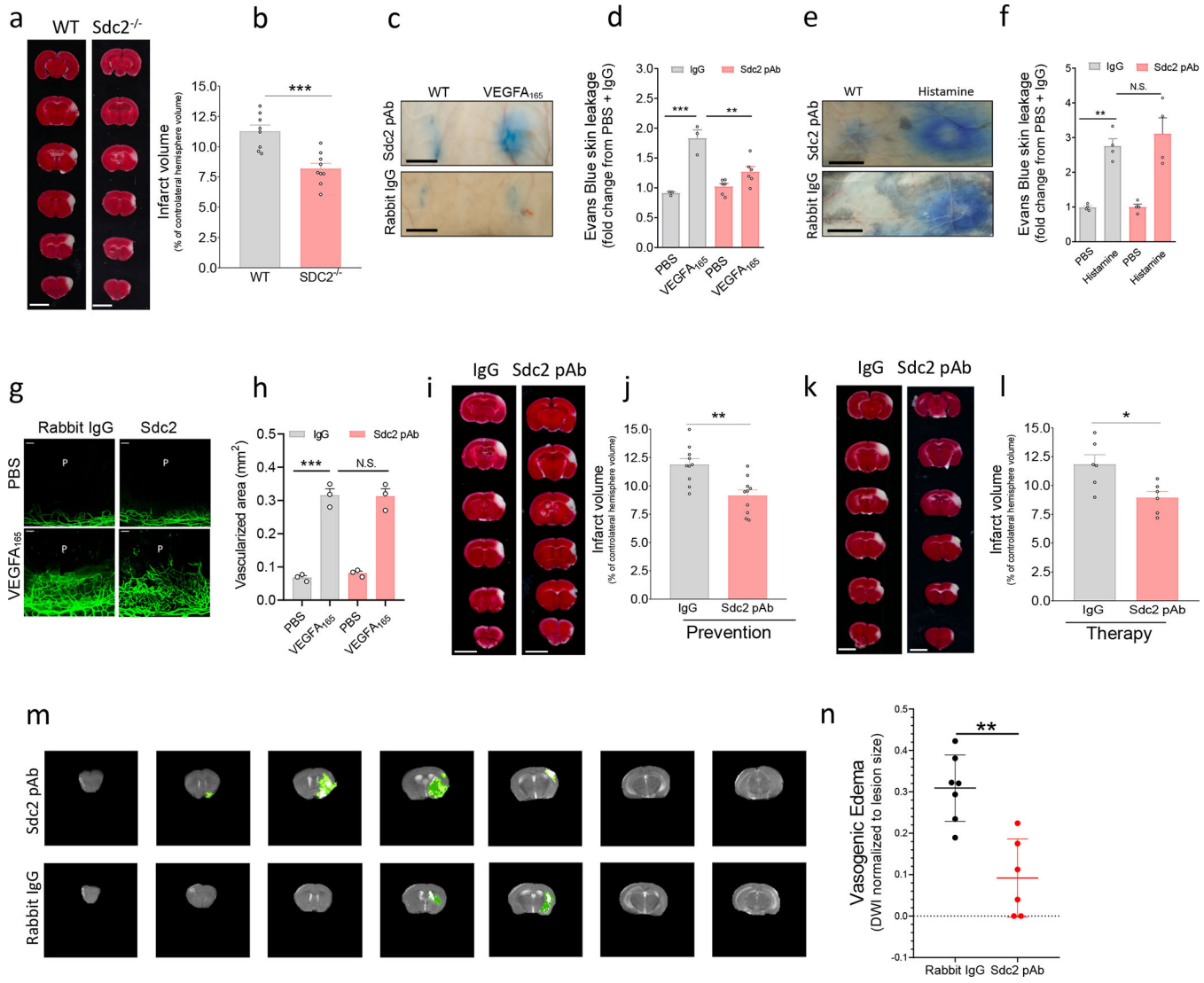

Fig. 4: Sdc2 deletion or treatment with an antibody that block Sdc2-DEP1 interaction confer neuroprotection in a mouse focal stroke model

a-b, TTC staining (24 hours stroke) and quantification of stroke infarct in wild type (WT) vs Sdc2$^{-/-}$ mice (n=8–9). **c-d,** $VEGFA_{165}$ -induced Evans blue dye leakage in the back skin of mice treated with rabbit IgG or Sdc2 pAb (I.V. injection of the antibody was 1.5 hours before $VEGFA_{165}$ stimulation)(n=3–6). **e-f,** Histamine -induced evans blue leakage in the back skin of mice treated with rabbit IgG or Sdc2 pAb (I.V. injection of the antibody was 1.5 hours before $VEGFA_{165}$ stimulation) (n=4). **g-h,** cornea pocket angiogenesis assay in mice treated with rabbit IgG or Sdc2 pAb (scale bars = 100 μm). The position of $VEGFA_{165}$ pellet (P) in the cornea is labelled in each cornea image **i-l,** TTC staining at 24 hrs and quantification of stroke size in mice treated with rabbit IgG or Sdc2 pAb before (prevention, panel i-j) (n=6) or after 1 hr from stroke (therapy, panel k-l) (n=10) stroke induction **m-n,** MRI compartmentalization analysis (see Material and Methods for details) allow to separate ischemic stroke core (white), penumbra (light green) edema (dark green) and quantification of vasogenic edema normalized to total stroke size (n=6–7).

Data are presented as mean values +/− SEM (standard error of the mean). In all figure panels, each dot represents a biological independent experiment (n). Statistical analysis was performed by unpaired two-tailed t-student test (panel b, j, l, n), one-way ANOVA with Sidak's multiple comparison test (panel d, f, h) (N.S. not significant, * $P<0.05$, ** $P<0.01$, *** $P<0.001$).

a

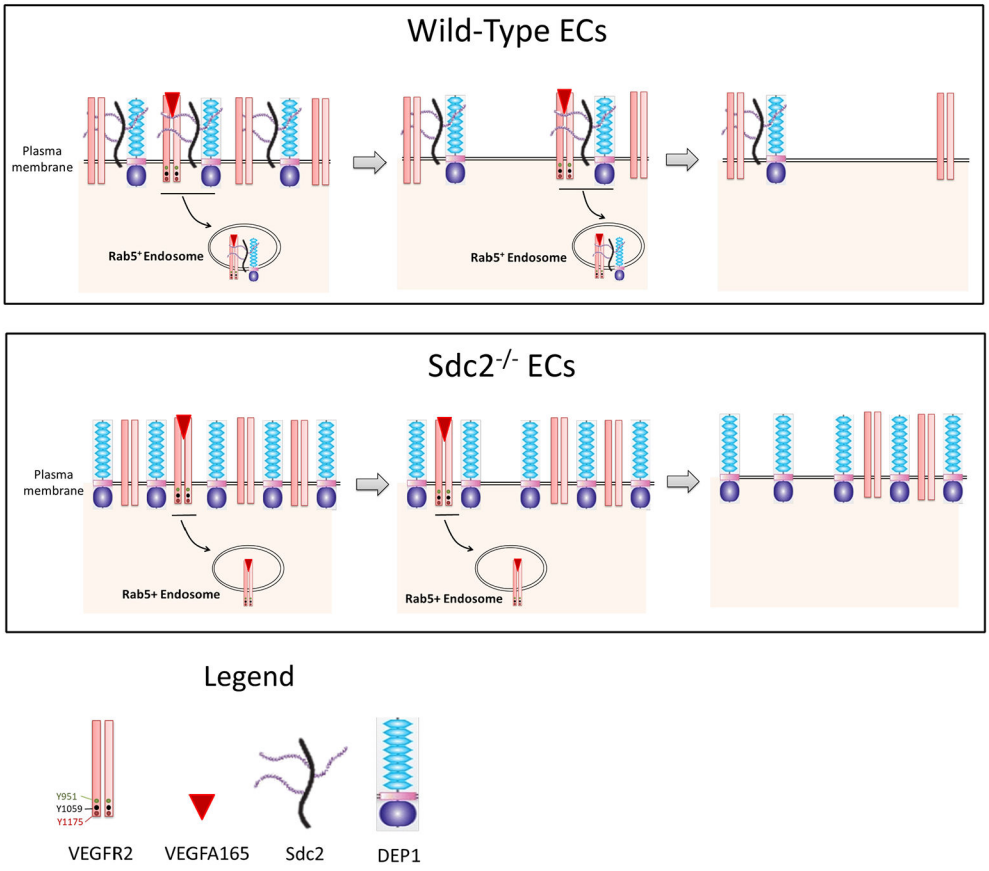

b

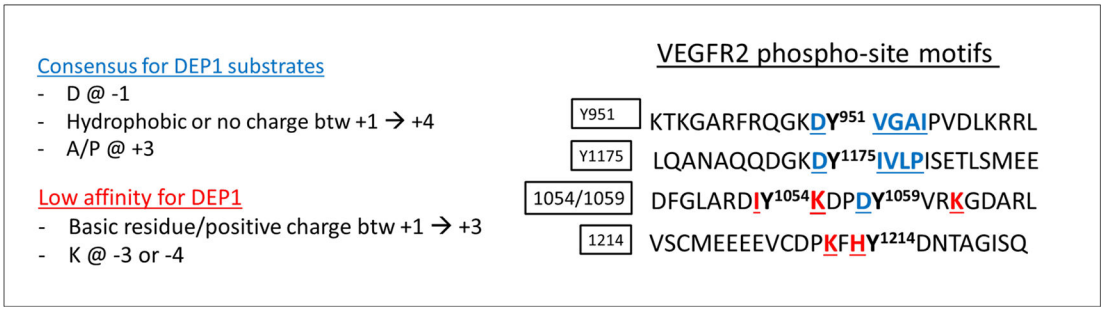

Fig. 5:

a, Proposed working model for accumulation of DEP1 at the cell surface and specific VEGFR2 Y951 dephosphorylation. The key control point is Sdc2-dependent endocytosis of DEP1. The two proteins normally exist in a heteromeric complex on the endothelial cell surface with Sdc2 internalization triggering DEP1 endocytosis thereby reducing its ability to dephosphorylate VEGFR2 Y951 site at the cell surface (top panel). In the absence of Sdc2, DEP1 inability to internalize leads to an increased stochiometric ratio of DEP1/VEGFR2 at the cell surface (lower panel), selective dephosphorylation of the VEGFR2 Y951 site, and

reduction in permeability response. **b,** DEP1 selectivity towards different phospho-tyrosine residues is influenced by the surrounding amino acids. Criteria were extrapolated from multiple studies assessing DEP1 target preferences [58–60]. Aspartic Acid at −1 position (D @ −1) is associated with increased tyrosine dephosphorylation by DEP1. Conversely, a lysine residue at −3 or −4 position (K @ −3 or −4) seems to inhibit DEP1 dephosphorylation. Additional criteria are reported in figure panel.